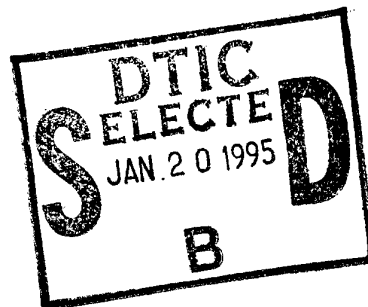# PROJECT

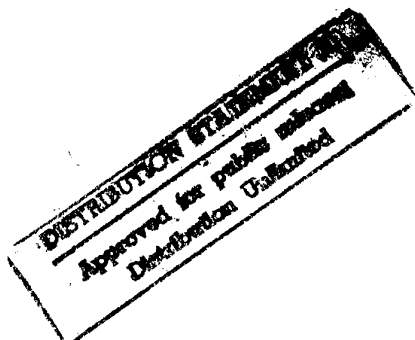## "SYNTHESIS AND APPLICATION

OF LARGE HETEROMETALLIC CLUSTER SYSTEMS"

CONTRACT NO: DA ƆA45 - 90 - C - 0034

Eighth Interim Report

November 1993

1.   *EXECUTIVE SUMMARY*

This report summarises the results obtained in the project to date
Fullerenes and Metallo-Fullerenes. This work was added in the
course of the project when Fullerenes became available in
larger quantities.

Results are as follows:

-   We were the first to observe and report optical nonlinearity
    of neat Fullerenes.

-   We were amongst the first to report and quantitatively
    describe optical limiting in Fullerenes.

-   We have studied the influence of metal substitution to
    control the nonlinear optical behaviour and improve optical
    limiting performance.

-   The use of Fullerenes as optoelectronic material in solar cells
    was assessed.

-   We have fabricated and investigated carbon nanotubes and
    find some unusual and interesting spectroscopic features.

2.   *STAFFING*

No major changes in staffing have occurred.

3.   *CONFERENCES, TALKS etc.*

The Trinity College Physics Group was actively involved in
organising a workshop on "Fullerenes for Photonics" in Austria,
at which they reported the results described below. Other
participants came from Germany, Austria and the U.K.

4.   *TECHNICAL DETAILS*

See reprints attached.

NONLINEAR OPTICAL RESPONSE OF
C_{60} AND C_{70} FULLERENES

W. J. BLAU* and D. J. CARDIN

*Department of Chemistry (*Department of Pure and Applied Physics)*
Trinity College, University of Dublin, Dublin 2, Ireland

The macroscopic preparation of novel conjugated allotropes of carbon, the Fullerenes, has become easy to achieve and commonplace, leading to widespread study of their physical and chemical properties. In this paper we review the nonlinear optical effects observed in Fullerenes to date. Both second and third order response has been studied and the results indicate that this class of materials is highly promising for optoelectronic applications.

1. Introduction

The interest in Fullerenes in both the scientific literature and the popular press appears unparalleled for a new group of molecules. It is also highly unusual for a novel chemical species to be first obtained in a laboratory as a result of research directed to understanding molecular species in stars and space.[1] Fascinating though these aspects undoubtedly are, and many remain tantalisingly unanswered, the explosion of interest among chemists and physicists followed the demonstration of a (relatively) simple macroscopic laboratory preparation.[2] In addition to a completely new field of chemical synthesis, which has only begun to be ploughed,[3,4] the Fullerenes have provided a wealth of interesting physico-chemical properties which have included (appropriately derivatised in some cases) conductivity and superconductivity, ferromagnetism, electroluminescence, and a range of nonlinear optical phenomena which form the subject of the present article. The subject has been reviewed from several standpoints, among the most useful of which reviews are references[5].

2. Properties and Structure

An undoubted factor responsible for the large number of laboratories currently involved in Fullerene research is the stability of at least the well known C_{60} and C_{70} molecules, whose resistance to thermal decomposition must extend to the temperature of the carbon arc discharges in which they are most frequently synthesised, coupled with high photostability. Stability of these species to electromagnetic radiation has been questioned in the literature, but both the conditions of formation,

1352   *W. J. Blau and D. J. Cardin*

and the numerous nonlinear optical studies made with high-power laser light showing no detectable degradation, testify to a high resistance to photochemical attack. It is however, worth noting that either when impure, or on certain chromatography column supports, there is evidence for light-induced decomposition, and that the oxidative stability is not particularly high. The available evidence to date also suggests that although not accessible in such high yields, the resistance of the higher Fullerenes to chemical attack or photolysis is similar.

Curiously for species available only recently, the structure of C_{60} (Fullerene-60) has been at least discussed for several years. In unconsciously prophetic publications in 1971,[6] Osawa and colleagues alluded to the aromaticity of such a molecule, while calculations on the molecular orbital structure of Fullerene-60 were made by Bochvar and collaborators shortly after, and by Davidson in 1981.[7] The suggestions of the now familiar structures, icosahedral Fullerene-60 and Fullerene-70 (D_{5h}); following experimental observation of these species in the mass spectrometer were first made by authors in Refs. 8 and 9 respectively. These structures are shown in Fig. 1.
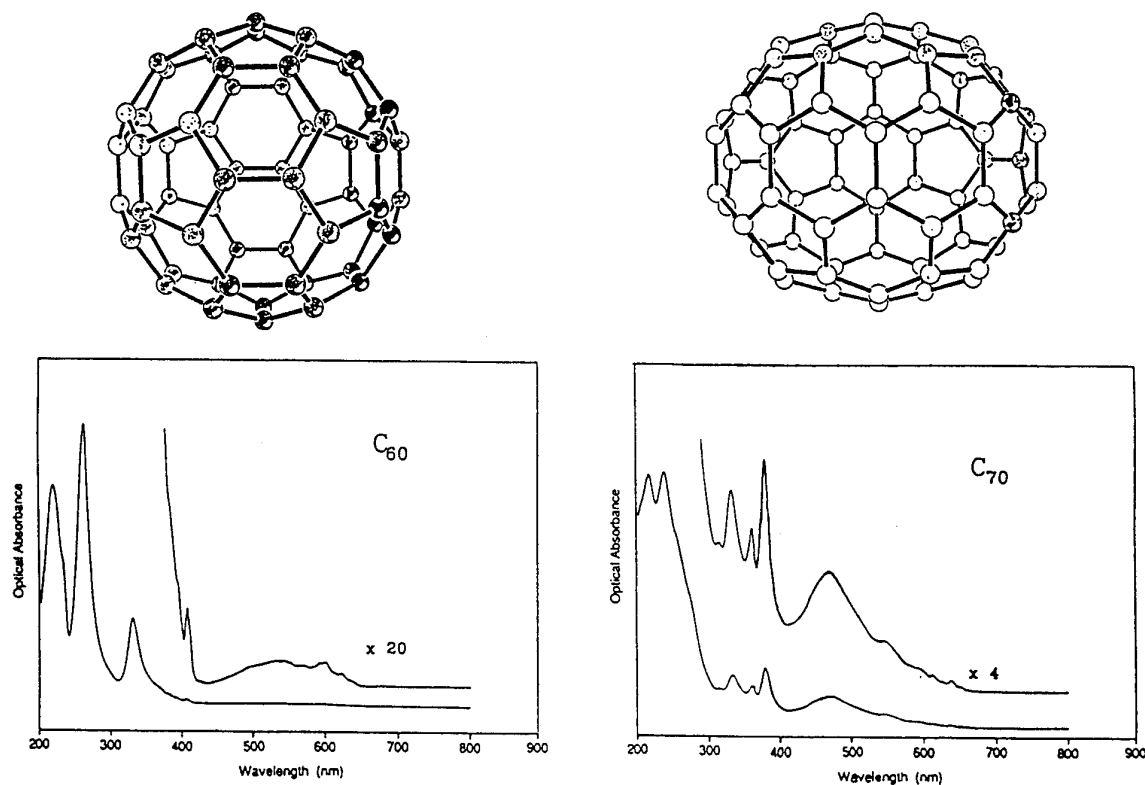

Fig. 1. Structure of C_{60} and C_{70} and their absorption spectra.

There is now a wealth of experimental evidence confirming beyond doubt the correctness of these early suggestions, among which the most convincing are spectroscopic,[10a] and X-ray structural data for a range of derivatives.[10b]

3. Nonlinear Optical Phenomena

The interaction of light with matter is usually characterised by several phenomena, such as light absorption, refraction, scattering and luminescence. In classical optics all of these were regarded as material properties, dependent on wavelength, but independent of intensity. The high light intensities which can be achieved with laser light however, are such that the electromagnetic field of the light can alter the optical properties of matter. Hence, the material characteristics also become a function of intensity. The study of such interactions is the field of nonlinear optics.[11]

As with all electromagnetic phenomena, optical interactions are governed by Maxwell's equations. The electric field of the light induces an optical dipole moment in the polarisable electrons of the material. This induced dipole moment in turn reradiates as an electromagnetic wave. For weak incident electric fields the induced polarisation P_{ind}, depends linearly on the electromagnetic field $E(\omega, k)$ of frequency ω and wave vector k:

$$P_{ind} = \chi^{(1)} E(\omega, k) \tag{1}$$

The linear susceptibility, $\chi^{(1)}$ is related to the complex dielectric constant ε,

$$\varepsilon(\omega) = 1 + 4\pi\chi^{(1)}(\omega) \tag{2}$$

where ε describes the classical low-power absorption and refraction.

When the incident electric field is larger, the induced dipole moment is no longer strictly linear in the field. The easiest description of such an induced nonlinear polarisation is in terms of a power series expansion of P_{ind}:

$$P_{ind} = \chi^{(1)} E(\omega, k) + \chi^{(2)} E^2(\omega, k) + \chi^{(3)} E^3(\omega, k) + \cdots \tag{3}$$

where $\chi^{(2)}$ and $\chi^{(3)}$ are the second and third order nonlinear susceptibilities.

On a molecular scalar this interaction is described by the polarisability α, and the hyperpolarisabilities β, γ, ... of the molecule in the local electric field E_{loc}:

$$P_{ind} = \alpha E_{loc}(\omega, k) + \beta E_{loc}^2(\omega, k) + \gamma E_{loc}^3(\omega, k) + \cdots \tag{4}$$

For simple spherical molecules the relationship between E_{loc} and the applied macroscopic field E is given by the Lorentz equation:

$$E_{loc} = (\varepsilon + 2)/3 \cdot E \tag{5}$$

In the most obvious case the hyper/polarisabilities of single molecules are assumed to be additive, and each molecule will contribute exactly once, hence macroscopic susceptibility and microscopic polarisability are interrelated with the density of molecules.

For a single frequency ω, the nonlinear terms in Eqs. (3) and (4) will generate polarisations at the harmonic frequencies 2ω, 3ω, ... This provides a means of

generating light at these higher frequencies, known as harmonic generation. More generally, if different light frequencies are employed, light may be generated at the sum and difference frequencies, known as parametric mixing. As is the case with any physical interaction, both energy and momentum conservation laws have to be observed. The frequency interactions described above, can therefore be interpreted by energy conservation. Momentum conservation is fulfilled on the wave vector scale, and as this is directly related to the linear refractive index, we also have to fulfil a refractive index matching condition (usually called phase matching).

All materials have a nonlinear response, and in particular those with a large number of delocalised electrons have comparatively high susceptibilities. The non-linear susceptibility is a tensor object and will in some manner reflect the symmetry of the material, thus reducing the number of independent tensor elements. For a material with inversion symmetry, such as C_{60} and C_{70}, which crystallise in a cen-trosymmetric space group, the second order susceptibility $\chi^{(2)}$ is identically zero; the third term however, $\chi^{(3)}$ is always nonzero. This term will manifest itself as an intensity-dependent absorption and/or refractive index. In molecular materials a range of possible nonlinear mechanisms exist arising from electronic, excitonic, or thermal effects. The actual mechanism may involve saturation of a particular tran-sition, induced changes in the dielectric constant arising from some excited state population, or possibly a thermally induced refractive index change. The specific contributions to the nonlinear response will depend on the linear optical properties of the material, the frequency of the light (photon energy), the intensity, and the temporal evolution. For a review of processes observed in conjugated molecules see Ref. 12.

Nonlinear optical response has been reported in C_{60} and C_{70} by a number of groups as cited below. Both second and third order effects have been observed in solutions and in thin films.

4. Second Order Nonlinear Response

Somewhat surprisingly two groups have reported second harmonic generation in C_{60} evaporated films.[13,14] These films are known to crystallise in a face-centred cubic array, and are therefore centrosymmetric. The exact reasons for the observations of second order effects have not been definitively established, though several explana-tions can be forwarded. X. K. Wang *et al.*,[14] have measured the bulk second order susceptibility $\chi^{(2)}_{zzz} = 2.1 \cdot 10^{-9}$ e.s.u. at room temperature with a pulsed Nd-YAG laser operating at 1.064 μm. This value is approximately 1.5 times larger than the susceptibility of quartz which is usually used as a reference material. It should be noted that quartz is not a particularly efficient second harmonic generating material, and some donor-acceptor substituted π-conjugated molecules possess substantially larger susceptibilities. The report by Y. Wang and L. T. Cheng[15] of second or-der nonlinearity of a C_{60}/N,N-diethylaniline charge transfer complex indicates that similar donor-acceptor structures can be made with Fullerenes, and therefore the

potential for enhancing the second order effect in Fullerene-containing molecules must be judged substantial. This is confirmed by the observation of X. K. Wang *et al.*, that Fullerene films can be poled in an electric field at elevated temperatures (~ 410 K) similar to substituted polymer films and the nonlinear susceptibility can be enhanced tenfold. These authors also observed that the growth of the nonlinear signal is proportional to the square of the film thickness. From this experiment one can conclude that the surface contribution to second harmonic generation (at the surface obviously centrosymmetricity is broken) is small. At a film thickness of 0.25 mm the second harmonic signal is more than three times larger than the surface effect and the general conclusion has to be that the observed signal results from a bulk response. This is also confirmed by the polarisation-dependence of the signal as reported in Refs. 13 and 14. The origin of a second harmonic signal in C_{60} can therefore only be a electric quadrupole or magnetic dipole contribution which is allowed in centrosymmetric materials or an impurity associated with the Fullerene species. At present, the latter explanation seems more plausible to the authors, in particular the poling procedure suggests that some complex is involved. Such an impurity could be traced to the extraction procedures.

Table 1. Comparison of Experimentally Obtained Third Order Nonlinearities in Fullerenes.

Molecule	Method	Wavelength	Nonlinearity	Ref.
C_{60} (film)	THG	1.064 mm	$\chi^{(3)} = 2 \cdot 10^{-10}$ esu	13
C_{60} (complex)	EFISH	1.91 μm	$\gamma = 7.5 \cdot 10^{-34}$ esu	15
C_{70} (solution)			$\gamma = 1.3 \cdot 10^{-33}$ esu	15
C_{60} (solution)	DFWM	1.064 μm	$\chi^{(3)} = 10^{-10}$ esu	16
C_{60} (film)	DFWM	1.064 μm	$\chi^{(3)} = 7 \cdot 10^{-12}$ esu	17
C_{60} (solution)	DFWM	532 nm	$\chi^{(3)} = 3 \cdot 10^{-7}$ esu	18
C_{60} (solution)	DFWM	1.064 μm	$\chi^{(3)} = 10^{-10}$ esu	19
C_{70} (solution)	DFWM	1.064 μm	$\chi^{(3)} = 5.6 \cdot 10^{-12}$ esu	20
C_{60} (solution)	SATAB	440 nm	$\chi^{(3)} = 6.8 \cdot 10^{-12}$ esu	21
		520 nm	$3.2 \cdot 10^{-11}$ esu	21
		580 nm	$1.7 \cdot 10^{-10}$ esu	21
C_{70} (solution)	SATAB	520 nm	$2.7 \cdot 10^{-10}$ esu	21
		580 nm	$2.0 \cdot 10^{-12}$ esu	21
		610 nm	$5.1 \cdot 10^{-11}$ esu	21

THG = Third harmonic generation; DFWM = Degenerate four wave mixing; EFISH = Electric field-induced second harmonic generation; SATAB = Saturable absorption.

5. Third Order Nonlinear Response

The initial publications in this area[13,16] have prompted much discussion and subsequent work.[15,17-20] Four different types of experiments have been performed — third
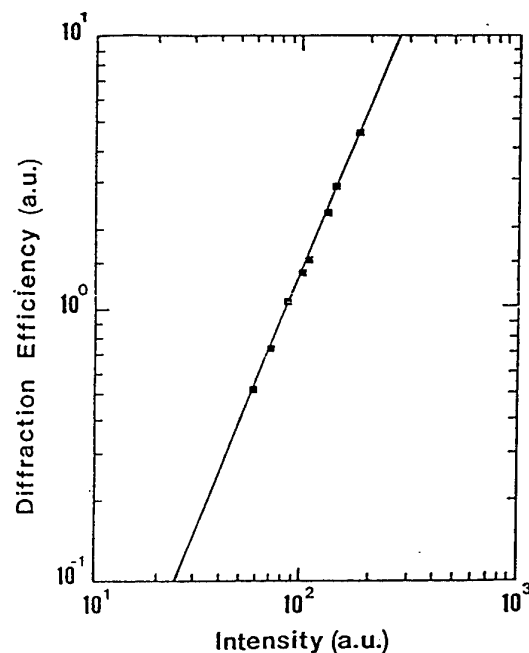
Fig. 2. Intensity dependence of the laser-induced grating diffraction efficiency in a 0.5 g L-1 solution of C_{60} in benzene. The solid line is a fit to a slope of 2, corresponding to a third order nonlinear process.

harmonic generation, degenerate four-wave mixing, nonlinear transmission and electric field induced second harmonic generation. A summary of the measured nonlinear susceptibilities and second hyperpolarisabilities is given in Table 1. Figure 2 shows an intensity dependence of the four-wave mixing signal using 50 ps Nd-YAG laser pulses at 1.064 μm in C_{60} solution in benzene.[16] The square-dependence of the diffraction efficiency of the laser-induced grating on incident intensity clearly indicates a nonresonant $\chi^{(3)}$ effect. In general, good agreement for the nonlinear susceptibility $\chi^{(3)}$, within experimental accuracies of the methods employed, can be observed in the transparency range of the material. $\chi^{(3)}$ values are in the range of 10^{-10} and $5 \cdot 10^{-12}$ esu. These values of the same order of magnitude as those of conjugated organic polymers[22] and both temporal and intensity responses are similar. The dispersion of both the third harmonic and the electric field induced second harmonic signals indicate that the primary resonance lies at the dipole-allowed transition of 2.8 eV in solid films. This is also confirmed by 2-photon resonant $\chi^{(5)}$ contribution at very high intensities, which was observed by Kafafi et al.[17] If the laser wavelength lies within one of the absorption bands of the material a resonant nonlinearity is observed, which is generally several orders of magnitude larger than the nonresonant phenomenon Shixiong Qian et al.[18] have observed a third order susceptibility as large as $3 \cdot 10^{-7}$ esu in both C_{60} and C_{70} solutions, using nanosecond Nd-YAG (second harmonic) pulses at 532 nm. With laser pulses which are one to two orders of magnitude shorter, F. Z. Henari et al.[21] have observed induced absorption in similar solutions yielding susceptibilities which are approximately four

orders of magnitude smaller. Figure 3 shows the transmission of a C_{60}-benzene solution at 608 nm as a function of incident laser intensity. The intensity where the transmission drops to the square root of its initial value gives the saturation intensity, which in turn is related to the imaginary part of $\chi^{(3)}$. Inserting the physical constants for a steady-state four-level system into the saturation intensity shows that the relaxation time of the excited state is substantially longer than the pulse width (> 200 ps). Therefore the excited state absorption can dominate the process and induced absorption is seen. This excited state absorption can be either in the singlet state which has a lifetime of 650 ps (Ref. 23) or, more plausibly, in the triplet state which has a lifetime of 103 μs and 91 μs for C_{70} and C_{60} respectively.[24] The large intersystem crossing yield (approximately 0.8) suggests that the nonlinearity in both Refs. 18 and 21 stem from a triplet state population.
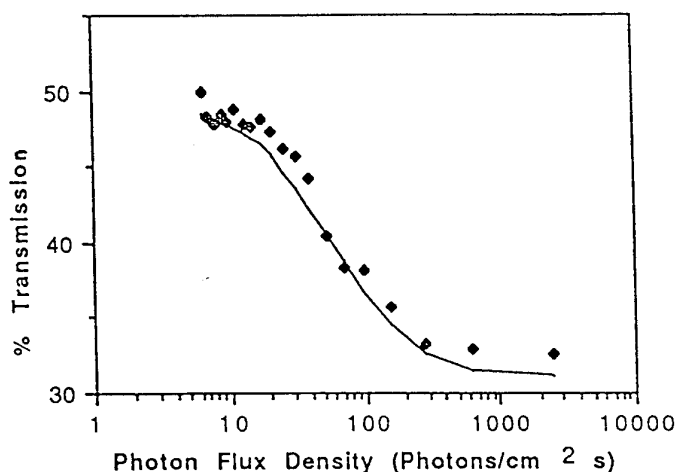

Fig. 3. Intensity dependence of the transmission of a 200 ps dye-laser pulse through a 0.5 g L^{-1} solution of C_{70} in benzene at 520 nm. Induced absorption is observed.

The origin for the nonresonant response has been attributed to the polarisability of the delocalised π-electrons in the Fullerene molecules. The quasispherical geometry of these systems provides a framework for these electrons which is similar to that of a semiconductor quantum dot.[25] Perturbation theory on the analytically calculated quantised energy levels of such a dot, yields an expression for the molecular nonlinearity which can give a order-of-magnitude estimate. More precise calculations using sum-over-states perturbation theory or other quantum chemical techniques should be employed to give a more quantitative description.

6. Summary and Conclusions

Fullerenes have been shown to have some very unusual second order and promising third order nonlinear optical response. Of particular interest will be Fullerene-containing molecular complexes which could be used in optoelectronic devices such

1358   *W. J. Blau and D. J. Cardin*

as second harmonic generators or integrated optical switches. The origins of both types of nonlinerity remain speculative, and their elucidation may have fundamental significance in understanding nonlinear optical effects in molecules.

Acknowledgments

References

1. J. R. Heath, Q. Zhang, S. C. O'Brien, R. F. Curl, H. W. Kroto, and R. E. Smalley *J. Am. Chem. Soc.* **109**, 359 (1987); H. W. Kroto, J. R. Heath, S. C. O'Brien, R. F. Curl, and R. E. Smalley, *Astrophys. J.* **314**, 352 (1987).
2. W. Kraetschmer, L. D. Lamb, K. Fostiropoulos, and D. R. Huffman, *Nature* **347**, 354 (1990).
3. P. J. Fagan, J. C. Calabrese, and B. Malone, *Acc. Chem. Res.* **25**, 134 (1992).
4. F. Wudl, *Acc. Chem. Res.* **25**, 157 (1992).
5. (a) H. W. Kroto, A. W. Allaf, and S. P. Balm, *Chem. Rev.* **91**, 1213 (1991); see also (b) special edition of *Acc. Chem. Res.* **25**, No. 3 (1992) containing 11 reviews of various aspects of Fullerene physics and chemistry.
6. E. Osawa, *Kagaku (Kyoto)* **25**, 854 (1970); *Chem. Abstr.* **74**, 75698v (1971); Z. Yoshida and E. Osawa, *Aromaticity*, Kagákudojin, Kyoto, 1971 (in Japanese).
7. D. A. Bochvar and E. G. Gal'pern, *Dok. Akad. Nauk. SSSR* **209**, 610 (1973); *Proc. Acad. Sci. USSR* **209**, 239 (1973); I. V. Stankevich, M. V. Nikerov, and D. A. Bochvar, *Russ. Chem. Rev.* **53**, 640 (1984); R. A. Davidson, *Theor. Chim. Acta* **58**, 193 (1981).
8. H. W. Kroto, J. R. Heath, S. C. O'Brien, R. F. Curl, and R. E. Smalley, *Nature*, **318**, 162 (1985).
9. J. R. Heath, S. C. O'Brien, Q. Zhang, Y. Liu, R. F. Curl, H. W. Kroto, and R. E. Smalley, *J. Am. Chem. Soc.* **107**, 7779 (1985).
10. (a) R. Taylor, J. P. Hare, Ala'a A. Abdul-Sala, and H. W. Kroto, *Chem. Commun.* 1423 (1990); (b) See for example *J. Am. Chem. Soc.* **113**, 8953 (1991), and references therein, and also J. M. Hawkins in Ref. 5(b).
11. Y. R. Shen, *The Principles of Nonlinear Optics* (John Wiley, 1984).
12. C. Maloney, H. Byrne, W. M. Dennis, W. Blau, and J. M. Kelly, *Chem. Phys.* **121**, 21 (1988).
13. H. Hoshi, N. Nakamura, Y. Maruyama, T. Nakagawa, S. Suzuki, H. Shiromaru, and Y. Achiba, *Jpn. J. Appl. Phys.* **30**, L1397 (1991).
14. X. K. Wang, T. G. Zhang, W. P. Lin, S. Z. Liu, G. K. Wong, M. M. Kappes, R. P. H. Chang, and J. B. Ketterson, *Appl. Phys. Lett.* **60**, 610 (1992).
15. Y. Wang and L.-T. Cheng, paper presented at "Workshop on Fullerites and Solid State Derivatives", Univ. of Pennsylvania, Aug. 2–3, 1991, unpublished, also *J. Chem. Phys.* **96**, 1530 (1992).
16. W. J. Blau, H. J. Byrne, D. J. Cardin, T. J. Dennis, J. P. Hare, H. W. Kroto, R. Taylor and D. R. M. Walton, *Phys. Rev. Lett.* **67**, 1423 (1991).
17. Z. H. Kafafi, J. R. Lindle, R. G. S. Pong, F. J. Bartoli, L. J. Lingg, and J. Milliken, *Chem. Phys. Lett.* **188**, 492 (1992).
18. S. Quian, G. Wang, J. Song, Y. Li, Y. Ye, and Y. Gu, submitted for publication in *Opt. Lett.* (1992).

19. Q. H. Gong, Y. X. Sun, Z. J. Xia, Y. H. Zhou, Z. N. Gu, X. H. Zhou, and D. Qiang, *J. Appl. Phys.* **71**, 3025 (1992).

20. S.-C. Yang, Q. Gong, Z. Xia, Y. H. Zhou, Y. Q. Wu, D. Qiang, Y. L. Sun, and Z. N. Gu, to be published in *Appl. Phys. B* (1992).

21. F. Z. Henari, J. Callaghan, W. J. Blau, and D. J. Cardin, accepted for publication in *Chem. Phys. Lett.* (1992).

22. H. J. Byrne and W. Blau, *Synthet. Metals* **32**, 229 (1990).

23. R. J. Sension, C. M. Phillips, A. Z. Szarka, W. J. Romanov, A. R. McGhie, J. P. McCauley, A. B. Smith, and R. M. Hochstrasser, *J. Phys. Chem.* **95**, 6075 (1991).

24. R. S. Becker, S. M. Hubig, T. J. Dennis, J. P. Hare, H. W. Kroto, R. Taylor, and D. R. M. Walton, submitted to *Phys. Lett.* (1992).

25. P. Horan and W. Blau, *Phase Transitions* **24–26**, 605 (1990).

26. S. V. Nair and K. C. Rustagi, submitted for publication in *Phys. Rev. Lett.* (1992).

27. L. M. Ramaniah, S. V. Nair, and K. C. Rustagi, unpublished manuscript (1992).

28. Y. Wang, G. F. Bertsch, and D. Tomanek, unpublished manuscript (1992).

29. K. Harigaya and S. Abe, *Jpn. J. Appl. Phys.* **31**, L887 (1992).

30. E. Westin and A. Rosen, in *Clusters and Fullerenes*, Proceedings of the Adriatico Research Conference, ICTP, Italy, 23–26 June 1992, ed. V. Kumar, T. P. Martin, and E. Tosatti.

31. Z. Shuai and J. L. Bredas, submitted to *Phys. Rev. B* (1992).

32. D. Neher, Max-Planck-Institut fuer Polymerforschung, Mainz, Germany; private communication.

33. R. J. Knize and J. P. Partanen, *Phys. Rev. Lett.* **68**, 2704 (1992).

34. Z. H. Kafafi, F. J. Bartoli, J. R. Lindle, and R. G. S. Pong, *Phys. Rev. Lett.* **68**, 2705 (1992).

35. L. W. Tutt and A. Kost, *Nature* **356**, 225 (1992).

36. D. Brandelik, D. McLean, M. Schmitt, B. Epling, C. Colclasure, V. Tondiglia, R. Pachter, K. Obermeier, and R. L. Crane, presented at the Symposium N: Electrical, Optical and Magnetic Properties of Organic Solid State Materials, MRS Fall Meeting, Boston, USA (1991).

37. Y. N. Han, W. J. Zhang, X. M. Gao, Y. X. Xia, G. Gu, W. C. Zang, Y. W. Du, and D. Feng, unpublished manuscript.

38. M. Sheik-Bahae, A. A. Said, T. H. Wei, D. J. Hagan, and E. W. van Stryland, *IEEE J. Quantum Electron.* **26**, 760 (1990).

Note Added

Since the submission of our manuscript a significant number of new results in the area of third-order optical nonlinearity of Fullerenes have been obtained. These have mainly been concerned with the theoretical calculation of the second hyperpolarisability with various quantum mechanical and quantum chemical methods.[26-31] In general, the theoretical predictions for the nonresonant nonlinearity appear to agree well, predicting a rather small susceptibility $\chi^{(3)}$ at zero frequency around 10^{-12}–10^{-11} esu for solid films and a second hyperpolarisability $\gamma = 2 \cdot 10^{-34}$ esu for C_{60}, and $8 \cdot 10^{-34}$ esu for C_{70}.

The calculated frequency dispersion of the nonlinearity shows multi-photon resonances above an incident photon energy of ~ 0.9 eV. This resonance behaviour has indeed been verified experimentally by D. Neher, G. Stegeman, *et al.*[32] The

agreement between theory and experiments in $\chi^{(3)}$ and γ appears satisfactory, at this point in time, both for thin films[17] and solutions.[15,16,32] It has been pointed out by various authors[33-34] that the values of the nonlinearities quoted in Ref. 16 are exactly a factor of 10^3 too large. This has been accounted for in the main text of this article and has indeed been confirmed by careful re-measurement and re-calculation of the value. A number of theoretical models predict that substituted Fullerenes, e.g. $C_{59}N$ and $C_{59}B$, will possess a substantially larger nonlinear response, both second- and third-order, than the unsubstituted molecules.[27,30]

Intensity dependent absorption, i.e., the resonant third-order nonlinearity of C_{60} and C_{70}, has been reported independently by several authors,[35,36] whose results and explanation of the effect are very similar to the one given in Paragraph 5. Both papers consider Fullerenes a promising material class for optical limiting and sensor protection with limiting thresholds which are lower than observed in currently used materials such as Carbon Black.

Recently, a highly surprising experiment has been reported by Han *et al.*[37] These authors have performed z-scan experiments on C_{60} thin films. They report giant $\chi^{(3)}$s of $1-3 \cdot 10^{-2}$ esu with continuous HeNe laser radiation at 633 nm, which they attribute to a two-photon resonance. It should be noted, that the effect observed is unusually large and that the technique employed by these authors is known to be very sensitive to thermal refractive index changes.[36,38]
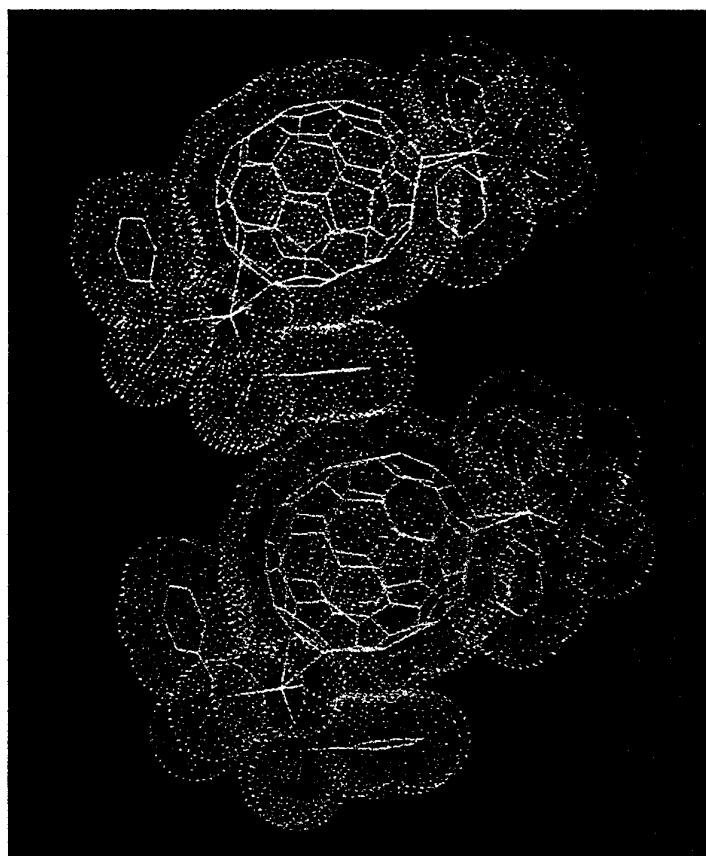
An organometallic fullerene (C_{60}) compound.

Two molecular representations of a C_{70} version of the same compound.

Carbon Chemistry and Buckyballs

In addition to diamond and graphite, chemists have recently discovered a new type of carbon material, where the molecules are spherical in shape. *Werner Blau* outlines the properties of these new compounds and writes about some potential applications, from solar cells to optical switching devices.

Like many aspects of modern life, science seems to progress in crazes. At least this is what the media pick up from the long, tedious and usually slow (but steady) progress made in the world's research laboratories. In recent years quite a few discoveries made the headlines: high temperature superconductors promised 100 per cent electrical power transmission and high speed magnetic levitation trains by the turn of the century, according to a front page of *Newsweek*: "Cold fusion" headlines promised unlimited supplies of environmentally friendly energy from electrolysis, until the whole thing proved a flop – or was it really? The scientific debate continues.

When news of a new molecular form of carbon broke in late 1990, a similar craze seemed to start, especially after a group in Bell Laboratories, USA, reported superconductivity in a doped version of the material. Sure enough, the number of publications started rising nearly exponentially in early 1992, but this time – had we learnt from past experience? – most scientists kept their sense and only a few spectacular, but reasonably realistic promises, appeared in TV programmes like 'Tomorrow's World'. Since then, progress on the new material, now called fullerene or buckyballs, has been steady and much new scientific understanding has been gained.

The involvement of a TCD group in this area started early in 1991 on a personal level. One of the researchers in my group, Mrs Anna Drury, gave me a photocopy of a brief article in *Chemistry in Britain*, I believe, describing a technique for preparing large quantities of fullerenes discovered by Krätschmer and co-workers at the MPI in Heidelberg, and its implication for a new aromatic three-dimensional chemistry. The Drurys had spent several years in Heidelberg and know the Krätschmers well. "Did I want contacts or some of this stuff?", Anna asked.

In the evening of the same day (!) my friend and colleague, David Cardin, now professor of inorganic chemistry at the University of Reading, showed me the same article and told me that he knew Prof. Harry Kroto, one of the other players in this field, from his days at the University of Sussex: "Should we start some research in this area?"

Fullerenes are electronically similar to some conjugated polymers which my research group was using in an EC project on fibre-optic switching, and so it was not difficult to start studying the nonlinear optical properties and potential applications of buckyballs. Harry Kroto gave us a few milligrams pretty fast, and a new research line for my group, and much international debate, started. This effort culminated in one of the first observations of sizeable nonlinearities in fullerenes.

Germ of an Idea

The origins of this new chemistry can be found in astronomy, an area of science which, at first glance, seems very remote from electronic applications. In the early 1970s, Walton and other radio astronomers observed assemblies of carbon atoms in interstellar matter. In an effort to simulate the high temperatures occurring inside stars and the subsequent generation of these carbon assemblies, an astrochemist from
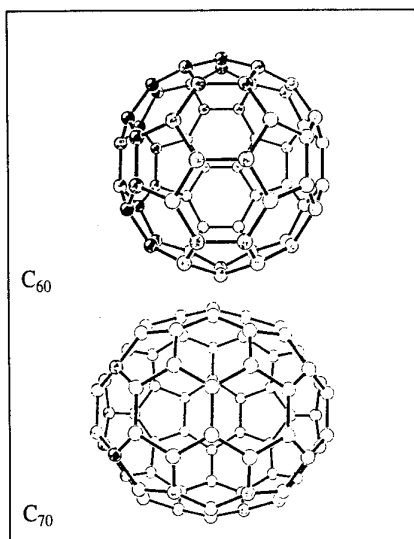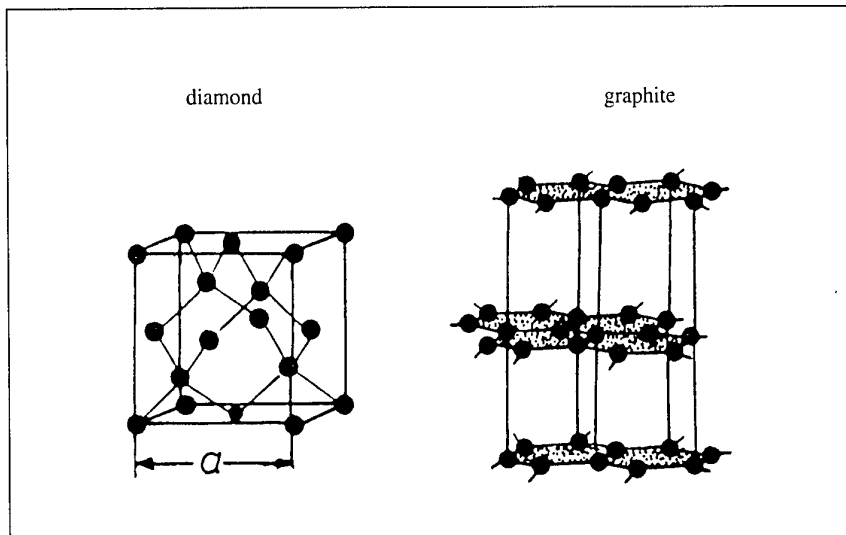
Molecular structure of the two most abundant fullerenes, C_{60} and C_{70}.

Atomic arrangements of the two 'classical' forms of carbon, diamond and graphite.

Sussex University, Harry Kroto, together with Prof. R.E. Smalley's group at Rice University, Houston, carried out some experiments on evaporating graphite with a high intensity pulsed laser source

When they analysed their results they found that they had generated an abnormally large fraction of material with 60 carbon atoms. There were no 'loose ends', so the molecule had to have some spatial structure which allows 60 carbon atoms to link up with each other. The solution turned out to be a truncated icosahedron which connects 60 equal points in the shape of a soccer ball. The mysterious C_{60} molecule had one carbon atom at each point and the molecular football was born. In addition to the C_{60} molecule, Kroto and co-workers also found C_{70} which has the shape of a molecular rugby ball. Since similar, large-scale structures were used by the American architect Buckminsterfuller in several spectacular geodesic dome shapes like the US pavilion at EXPO'67 in Montreal, the names buckyballs and fullerene were given to this new class of carbon molecules.

Although Kroto's laser experiments in 1985 attracted much attention, due to the aesthetic and fundamental interest in such novel molecules, the laser evaporation produced only a few molecules per laser shot. The practical breakthrough occurred in 1990 when Krätschmer and co-workers observed large quantities of fullerene in soot produced by an electrical arc discharge in an inert helium gas atmosphere.

In this technique, graphite electrodes are burnt in 100 mbar of helium and the resultant soot is collected. The inert gas atmosphere provided by the helium prevents oxidation taking place and thus the formation of CO and CO_2, which occurs in an ordinary fireplace. The low pressure serves to keep the vaporized carbon in the burning area long enough for the atoms to assemble. The complex conditions required mean that fullerenes are not normally found on this planet, apart from one location in Siberia where obviously just the right conditions occurred at some prehistoric time.

The small molecular fractions in the soot can be dissolved in toluene and separated into C_{60}, C_{70} and C_{84} fractions by standard laboratory chromatography (HPLC). The apparatus in our laboratory employs a 120 amp DC welding power supply and a simple single stage rotary pump. Gram quantities of fullerene can in principle be obtained on a weekly timescale and any kind of carbon can be used in the arc: charcoal and even peat have been used as starting materials.

But how can we be sure that buckyballs are what we think they are? With large quantities of the materials available now, a multitude of spectroscopic tests can be used to confirm the chemical structure. Nuclear magnetic resonance (NMR), X-ray crystallography, infrared absorption (FMR), Raman spectroscopy, and scanning tunnelling and electron microscopy can all be used. A number of inorganic and organic chemical compounds incorporating fullerenes have also been synthesised, like the organoplatinum compound shown here. The spherical shape of C_{60} has now been clearly verified, with an outer diameter of circa 10Å (10^{-9}m) including the π-electron shell surrounding the carbon skeleton.

An obvious feature of fullerenes, both in solution and as evaporated thin films on glass, is their strong colour, which ranges from yellow/orange to purple. This tells us immediately that the electronic structure, and thus the optical response, will be substantially different from the two conventional forms of carbon, graphite and diamond, which look black and transparent, respectively. Diamond is a very hard, insulating crystal, whereas graphite is soft and electrically conducting. The physical properties of fullerenes might be expected to lie somewhere in between.

In fact, the molecular electronic structure had been calculated by Davidson in 1981, long before any such molecule could be measured, and in a paper in *Theoretica Chemica Acta* he predicted the pyrolytic route which Krätschmer *et al.* found nearly 10 years later. Davidson's theories and subsequent calculations using various other quantum-chemical methods predicted the electronic structure, and hence the colour, of fullerene quite exactly.

In the solid form (fullerenes can be evaporated onto virtually any substrate using a standard commercial evaporation plant) they form simple crystallites, such as a face-centred cubic structure for C_{60}, due to the high symmetry of the molecular unit. More sophisticated growth techniques have yielded actual single crystals of millimetre and even centimetre size. In electron microscopy further related carbon shapes have also been found such as atomic-sized tubes (so called nanowires) and molecular 'onion' shapes.

Good for Something?

It is obviously not reasonable to expect large-scale applications for fullerenes to have emerged after only two years, but there is lots of potential in a wide range of areas. Initial ideas for applications of fullerenes relied mainly on their shape. If the π-electrons, which 'stick-out' from the carbon atoms can be saturated with hydrogen or fluorine, we could get microscopic spheres of polyethylene ($C_{60}H_{60}$) or teflon ($C_{60}F_{60}$) which should be extremely good lubricants.

Alternatively, if one could incorporate other atoms or molecules inside the carbon framework, the molecule could be used to carry the passenger atom/molecule to a specific site and release it there, say by a zap with an ultraviolet laser. Larger fullerenes could even carry photoactive drugs to tumour sites inside the body and destroy the tumour locally upon release.

Unfortunatelly, all these ideas proved chemically extremely difficult. It is very hard to keep more than just a few (say six) other atoms bound to the C_{60} sphere, and incorporating even simple ions (Li, K) in large quantities, although possible, is not yet feasible.

At first sight, the electrical properties of fullerenes look modest. C_{60} is an n-type semiconductor, with fairly low electrical conductivity, due to the large band gap, and low carrier mobility. C_{70} is a little better due to its smaller band gap and recent experiments in our laboratory, carried out by graduate students
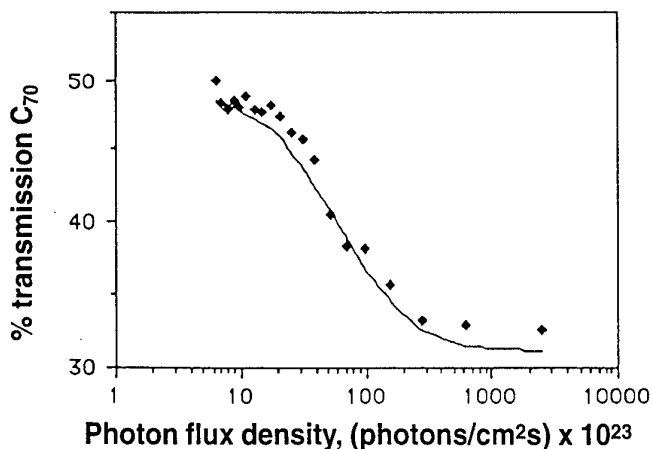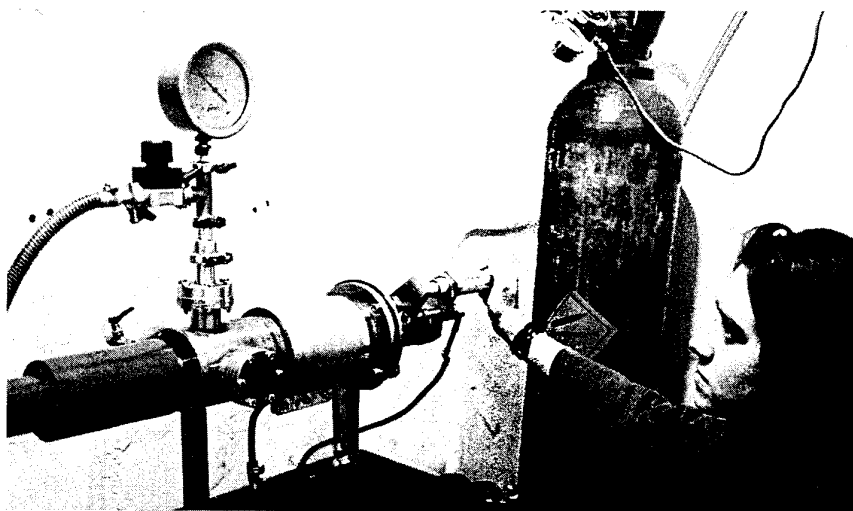
Figure 1: Optical transmission of the fullerene sample as a function of increasing light intensity, showing optical limiting response.

The fullerene generator at TCD. The carbon rods are burnt inside a water-cooled stainless steel chamber.

Seamus Curran and Joe Callaghan, show that C_{70} forms a pretty respectable Schottky diode when put in contact with heavily n-type doped silicon. Moreover, when daylight is shone onto this fullerene diode it produces a photovoltaic signal of about 0.2V. Although the efficiency of this solar cell is low, at present about 0.1 per cent, it offers an exciting perspective. If we can deposit large areas of this material on conducting polymer films, we could fabricate solar cell sheets to cover slates, or a whole roof, and thus generate electricity in remote areas at fairly low cost – though the efficiency of the device would need to be increased by an order of magnitude before this would be practical.

Superconductivity is another area where fullerene attracted much attention from the international scientific community. In April 1991, Hebard and co-workers at Bell Laboratories in the USA reported superconductivity in potassium-doped C_{60} at a 'critical temperature' (T_c) of 18K (-255°C). (Superconductors lose their electrical resistivity below T_c, when an electrical current can flow with no loss.) Doping with other alkali metals raised this critical temperature to approx. 40K (-233°C), the highest critical temperature

observed to date in any (nearly) organic system. This would have attracted much more attention a few years ago, had inorganic superconducting ceramics not been discovered by Bednoz and Mueller with a T_c up to 130K (-143°C).

Nevertheless, the question of why superconductivity occurs in these materials is of great fundamental interest. Understanding the nature of the superconducting mechanism might tell us how to increase T_c. The alkali metal doping used to date, however, is not really practically feasible as alkali metals tend to ignite spontaneously in air.

As mentioned above, the major work carried out in my research group is on applications of nonlinear optical materials and processes, and this was how we got into this new field. Nonlinear optics is a relatively new brand of optics, concerned with changes in the optical properties of matter induced by external electromagnetic fields. Obvious applications are in optical communications where, for example, a microwave drive signal modifies the optical path of one arm of a Mach-Zehnder interferometer, thereby functioning as an electro-optic modulator. More advanced concepts involve using light beams to modify

the refractive index in part of a device, leading to all-optical switching devices where one light beam controls a second one at extremely high speed (50 GHz).

When our group had a look at fullerenes, we found a strong, very fast response as expected. The most striking observation which we made in the early stages of our research – and later found out that at least four other major laboratories in the USA had found as well – was that a strong light pulse propagating in fullerene modifies its own propagation path through the nonlinear refractive index. This manifests itself in the phenomenon of optical limiting (Figure 1): the ability to let light through the sample decreases as the intensity increases. Hence, bright light pulses will be blocked while weak ones won't.

I was particularly intrigued to find last August, during a lecture tour of the USA, that the materials laboratory of the US Air Force in Dayton, Ohio, had a large group of scientists working in exactly this area for sensor protection. Armies use pulsed lasers for many applications, such as range finders, and also for 'switching off', i.e. destroying highly sensitive sensors on satellites. A filter which protects a sensor against high power light is therefore of direct interest to the military, and fullerenes appear to perform this optical limiting function better than the conventional materials used in this context, e.g. carbon-black particles.

The same effect could obviously also be employed in a civilian context especially when one intense light beam switches a weak signal beam on or off. By placing a nonlinear material like fullerene between two parallel reflecting mirrors, the same effect can also be used to impose a weak image onto a strong laser beam. Such a device is called a spatial light modulator (SLM), and can be used in display applications for advertising, large scale TV picture projection, or to input images into an optical computer. Our group and the NMRC in Cork are jointly experimenting with an SLM as an optical amplifier for an EOLAS strategic research project, and fullerenes may be the answer here as well! ∎

References
The total number of publications on fullerene now exceeds 1,000, including several overview articles. Most are listed in an electronic mail bibliography service provided free of charge by the University of Pennsylvania. For instructions on how to use the bibliography send the message 'INTRO' to the INTERNET address: BUCKY@SOL1.LRSM.UPENN.EDU

Werner Blau is associate professor of materials science at the Physics Department, Trinity College, Dublin, and director of the Materials Ireland polymer unit.

Large Infrared Nonlinear Optical Response of C_{60}

W. J. Blau and H. J. Byrne[a]

Department of Pure and Applied Physics, Trinity College, Dublin 2, Ireland

D. J. Cardin

Chemistry Department, Trinity College, Dublin 2, Ireland

T. J. Dennis, J. P. Hare, H. W. Kroto, R. Taylor, and D. R. M. Walton

School of Chemistry and Molecular Sciences, University of Sussex, Brighton BN1 9QJ, United Kingdom

(Received 22 May 1991)

C_{60} buckminsterfullerene exhibits a large ultrafast third-order nonlinear optical response. Degenerate four-wave-mixing measurements in C_{60}-benzene solutions were performed using 50-psec pulses at 1.064 μm. The magnitude of the nonlinear susceptibility per C_{60} molecule is $|\gamma| = 1.5 \times 10^{-42}$ m^{5}V^{-2} and of the same size as that observed in polydiacetylene. In contrast to conjugated polymers, however, a dominant positive real part of the nonlinearity is found, 3 times larger than the imaginary component. The nonlinear response can be described within the model of a free electron in a spherical box, confirming the complete delocalization of electrons on the C_{60} molecule.

PACS numbers: 42.65.-k, 33.20.Ea, 36.90.+f

Confinement of free or quasifree electrons on a nanometer scale has received considerable interest in optics recently [1]. In semiconductor nanoparticles, for example, carrier confinement leads to a singularity in the density of states at the band gap which in turn gives rise to an enhanced nonlinear optical response near the associated optical transition compared with nonconfined materials [2]. Such particles are commonly termed quantum dots. On the other hand, conjugated polymers such as polyacetylene and polydiacetylene show sizable ultrafast nonlinearities due to the one-dimensional nature of the delocalized π electrons [3]. Fullerenes [4–9] also possess highly delocalized electrons and so are expected to exhibit nonlinear optical behavior similar to conjugated polymers. In addition, however, the three-dimensional nature of the particles should also be apparent in this response. In this Letter we report the observation of infrared nonlinear optical response of C_{60}-buckminsterfullerene-benzene solutions which shows some similarity with that of conjugated polymers. As a result of a dominant real part of the nonlinearity and the relatively small size of the molecule, however, more favorable solid-state properties can be expected, making this class of materials interesting candidates for nonlinear optical devices.

C_{60} buckminsterfullerene was prepared and purified as described in the literature [8,9]. Magenta solutions up to a maximum concentration of 500 mg/L were prepared in benzene. The absorption spectra of the samples are complex consisting of a series of closely overlapping peaks between 450 and 700 nm with a first absorption maximum near 593 nm. In general, the similarity of this spectrum with that of 3-BCMU polydiacetylene in chlorobenzene should be noted [10].

Nonlinear optical measurements were performed using the forward degenerate four-wave-mixing technique as described elsewhere [11]. The laser used was a passively

mode-locked amplified Nd-doped yttrium-aluminum-garnet laser emitting 50-psec pulses at 1.064 μm of up to 5 mJ energy. This technique is based on diffraction from nonlinear optically induced transient gratings and allows the magnitude of the nonlinear optical response to be measured. The observed response corresponds to a modulation of the material's refractive index associated with the light-induced polarization of the delocalized electrons. In centrosymmetric materials, such as buckminsterfullerene, the induced polarization can be described by [12]

$$P_{\text{ind}} = \varepsilon_0 \chi^{(3)} E^3, \qquad (1)$$

where $\chi^{(3)}$ is the third-order nonlinear susceptibility, E the applied electric field of the laser pulse, and ε_0 the permittivity of free space. Therefore $\chi^{(3)}$ provides a measure of the magnitude of the cubic nonlinear response. In molecular systems it is usual to normalize the nonlinearity to one molecule, in which case one obtains the hyperpolarizability γ from

$$\gamma = \chi^{(3)}/NL^4, \qquad (2)$$

where N is the density of molecules per unit volume and L is the Lorentz field factor associated with the shielding of the electric field experienced by the molecule in its local environment. Experimentally one observes the diffraction efficiency η of the laser-induced grating which corresponds to $(P_{\text{ind}}/E)^2$. The cubic nonlinear susceptibility can be derived by comparing the intensity dependence of the diffraction efficiency with that of a material of known nonlinear response such as neat benzene ($\chi^{(3)} = 2 \times 10^{-21}$ m^{2}V^{-2}) [9]. As the intensity I is proportional to E^2, η depends quadratically on I as shown in Fig. 1 for a 15-mg/L solution of C_{60} buckminsterfullerene. This confirms that the nonlinear response originates from a third-order susceptibility. By accounting for
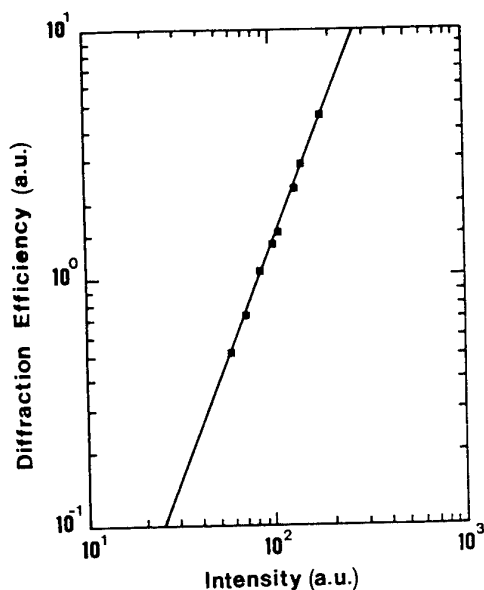
FIG. 1. Intensity dependence of the diffraction efficiency of the laser-induced grating in a 15-mg/L solution of C_{60} buckminsterfullerene in benzene. The solid line is a fit with a slope of 2, typical of a third-order nonlinear susceptibility.

FIG. 2. Concentration dependence of the nonlinearity of C_{60} buckminsterfullerene in benzene.

concentration effects as described below, the magnitude of the hyperpolarizability of a C_{60} molecule can be calculated and is found to be $|\gamma| = (1.5 \pm 0.3) \times 10^{-42}$ m^{5}V^{-2}. It is again interesting to note that this value is similar to that of polydiacetylene solutions ($|\gamma| = 2.0 \times 10^{-42}$ m^{5}V^{-2}) [13]. The temporal decay of the nonlinearity was investigated with the same laser using a phase-conjugation setup [12]. It was found to decay within the pulse width of 60 psec.

The optical nonlinearity consists of both a real and an imaginary component. The imaginary part accounts for changes in absorption (saturable or induced) whereas the real part constitutes a change in refraction. Organic solvents such as benzene only possess a real positive nonlinear response originating from the optical Kerr effect [12]. By observing the dependence of the total nonlinear response of a solution as a function of solute concentration it is possible to derive both the sign and magnitude of the real part and the magnitude only of the imaginary part of γ [13]. Figure 2 shows the dependence of the square of the susceptibility on the concentration, which should be a parabola. Obviously the real part of the nonlinearity has the same sign as the solvent response and is therefore positive. At high concentrations a leveling off of the concentration dependence can be seen, which is frequently observed in molecular systems and indicates a strong tendency for aggregation of the solute. By fitting the dependence as described in Ref. [13] one obtains a ratio of the real to the imaginary part as $\gamma_R/\gamma_I = 3.2$, i.e., the real part dominates. This behavior is different from that of conjugated polymers where the imaginary com-
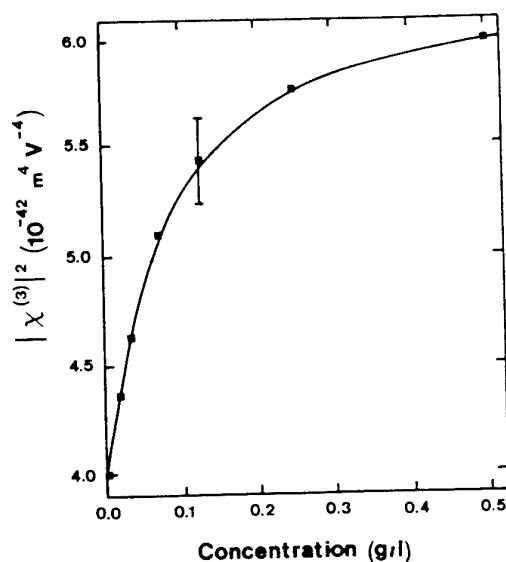
ponent is usually at least the same magnitude as the real [13].

The similarity between the nonlinear optical behavior of C_{60} buckminsterfullerene and typical conjugated polymers may be attributed to the fact that the electrons in both systems are substantially delocalized. A simple model for the optical response of conjugated carbon chains was proposed by Rustagi and Ducuing [14]. The molecules were treated as one-dimensional boxes containing delocalized π electrons. This so-called "free-electron" model predicts a large real nonlinearity away from optical absorption bands. Because of the fact that imaginary components sometimes dominate in conjugated polymers, this model does not always lead to a quantitative understanding of the nonresonant processes in polymers. It is simple to extend this model to describe delocalized electrons on a spherical surface. By solving the Schrödinger equation of this system we obtain an expression for the energy levels of the electrons which correspond exactly to the simple one-dimensional solution. Following the procedure outlined in Ref. [14] one can calculate the hyperpolarizability of the sphere by fourth-order perturbation theory as

$$\gamma = \frac{128L^{10}}{a^3 e^2} \sum_{n=1}^{N} \left(-\frac{2}{9\pi^6 n^6} + \frac{140}{3\pi^8 n^8} - \frac{440}{\pi^{10} n^{10}} \right), \quad (3)$$

where L is the circumference of the sphere, a the width of the electron shell, e the electron charge, and N the total number of delocalized electrons ($N = 60$). γ is completely real and, for large N, positive. Taking a circumference of $L = 22$ Å derived from standard bond lengths and spherical geometry and an electron shell width of 2.5 Å into account, the position of the first absorption max-

imum can be calculated to be 550 nm and the hyperpolarizability to be $\gamma = 2 \times 10^{-42}$ $m^5 V^{-2}$ from Eq. (3). This is in good agreement with the experimental data, and therefore suggests the existence of a delocalized π-electron system around the surface of the nearly spherical C_{60} buckminsterfullerene as also indicated by the increase in electrical conductivity and the detection of superconductivity in doped material [15]. The increase in the ratio of the real to the imaginary part of the nonlinearity compared with that in conjugated polymers is consistent with a decrease in the electron-vibration coupling characteristic of a more rigid spherical molecular system. Such a feature is most desirable for applications in integrated nonlinear optical devices. In addition, the magnitude of the nonlinearity in the solid state can be extrapolated from the solution data and is expected to be approximately 10^{-16} m^2/V^2 ($\approx 10^{-8}$ esu). This is a remarkably large nonresonant value which should exceed those obtained from conjugated polymers. Initial measurements of nonlinear prism coupling in thin films of C_{60} yield a value $\chi^{(3)} = (6 \pm 4) \times 10^{-8}$ esu in the solid state, which confirms the predictions from our solution data.

[a]Now at Max-Planck-Institut für Festkörperforschung, Stuttgart, Germany.

[1] For a recent review see, e.g., Y. Wang and N. Herron, J. Phys. Chem. **95**, 525 (1991).

[2] P. Horan and W. Blau, Phase Transitions **24-26**, 605 (1990).

[3] *Organic Molecules for Nonlinear Optics and Photonics*, edited by J. Messier, F. Kajzar, and P. Prasad, NATO Advanced Study Institutes, Ser. E, Vol. 195 (Kluwer Academic, Dordrecht, 1990).

[4] H. W. Kroto, J. R. Heath, S. C. O'Brien, R. F. Curl, and R. E. Smalley, Nature (London) **318**, 162 (1985).

[5] H. W. Kroto, Science **242**, 1139 (1988).

[6] For a recent review see H. W. Kroto, A. W. Allaf, and S. P. Balm, Chem. Rev. (to be published).

[7] W. Krätschmer, K. Fostiropoulos, and D. R. Huffman, Chem. Phys. Lett. **170**, 167 (1990).

[8] W. Krätschmer, L. D. Lamb, K. Fostiropoulos, and D. R. Huffman, Nature (London) **347**, 354 (1990).

[9] R. Taylor, J. P. Hare, A. K. Abdul-Sada, and H. W. Kroto, J. Chem. Soc. Chem. Commun. **1990**, 1423.

[10] *Polydiacetylenes*, edited by D. Bloor and R. R. Chance, NATO Advanced Study Institutes, Ser. E, Vol. 102 (Martinus Nijhoff, Dordrecht, 1985).

[11] P. Horan, W. Blau, H. J. Byrne, and P. Berglund, Appl. Opt. **29**, 31 (1990).

[12] Y. R. Shen, *The Principles of Nonlinear Optics* (Wiley, New York, 1984).

[13] H. J. Byrne and W. Blau, Synth. Met. **37**, 231 (1990).

[14] K. C. Rustagi and J. Ducuing, Opt. Commun. **10**, 258 (1974).

[15] A. F. Hebard, M. J. Rosseinsky, R. C. Haddon, D. W. Murphy, S. H. Glarum, T. T. M. Palstra, A. P. Ramirez, and A. R. Kortan, Nature (London) **350**, 600 (1991).

Intensity-dependent absorption and resonant optical nonlinearity of C_{60} and C_{70} solutions

F. Henari [a], J. Callaghan [a], H. Stiel [b], W. Blau [a] and D.J. Cardin [c]

[a] *Physics Department, Trinity College, University of Dublin, Dublin 2, Ireland*
[b] *Institut für Nichtlineare Optik und Kurzzeitspektroskopie, W-1199 Berlin, Germany*
[c] *Chemistry Department, Trinity College, University of Dublin, Dublin 2, Ireland*

We present the optical response of solutions of C_{60} and C_{70} fullerenes to high-intensity visible laser pulses. A decrease of the transmission with increasing input intensity is observed at different wavelengths. The measurements are compared with simulations using a rate equation model. Excited-state absorption cross sections are evaluated and used to calculate the imaginary part of the resonant nonlinear susceptibility $\chi^{(3)}$.

Nonlinear optical processes have been proposed for a variety of applications including optical phase conjugation, all-optical switching, sensing and optical sensor protection [1]. In these areas, materials possessing a low saturation intensity are of particular interest, since this is related to a high nonlinearity.

The recent synthesis and characterization of the all-carbon molecule buckminsterfullerene by Krätschmer et al. [2] has opened a door to detailed studies of these new materials. Many interesting properties such as superconductivity [3], photoconductivity [4], electroluminescence [5], and nonlinear optics [6] have been reported. Several groups [6] have demonstrated a close similarity between the nonlinear behaviour of the fullerene family and typical conjugated organic molecules. They have attributed this behaviour to the delocalization of the π electrons in both types of systems. This similarity is of particular interest since organic materials are widely used for Q switching and mode locking using saturable absorption as the switching mechanism [7].

In most materials, the transmission increases with the incident intensity. However the decrease of the transmission with increasing intensity can be observed when the absorption cross section of the

ground state is smaller than that of the excited state (reverse saturation, induced absorption). This phenomenon has been observed experimentally in semiconductors [8], a number of dyes [9] and organometallic materials [10]. This effect should prove extremely useful in making devices such as optical limiters for the protection of eyes, optical sensors and switches.

Here we report the observation of intensity dependent absorption in fullerenes and present a model for the mechanism. Measurements were carried out on solutions of C_{60} and C_{70} in benzene using 5 ns pulses at different wavelengths. Information regarding the molecular states responsible for the excited-state absorption cross sections can be determined from population distributions of a six-level system model. From a comparison of the experimental data and theoretical curves, the excited-state absorption cross section responsible for this effect can be estimated. The intensity dependence of the transmission is used to calculate the value of the imaginary component of the third-order nonlinear susceptibility $\chi^{(3)}$.

The samples were prepared and purified as described in the literature [2,11]. Solutions of concentration 10^{-5} M were prepared in benzene. The linear absorption spectra of these samples agree with those published in ref. [2].

Correspondence to: F. Henari, Physics Department, Trinity College, University of Dublin, Dublin 2, Ireland.

The experimental technique used in these measurements is equivalent to that described in ref. [12] (Z-scan technique, open aperture) and shown in fig. 1. The experiments were performed with a tunable dye laser (molectron DL-100) pumped by a low-pressure (molectron UV-300 N_2) laser giving pulses of 5 ns duration and typically 40 µJ energy. Different dyes were used covering ranges between 440 and 610 nm. The transmission of C_{60} and C_{70} as a function of the sample position, z, was measured with respect to the focal plane. A lens of 5 cm focal length was used giving a typical power density of 10^6 W/mm^2 in the focus, and each data point was averaged over 30 shots at a repetition rate of 1 Hz. Different repetition rates were used, and within the limits of experimental error no significant differences were observed, thus indicating that no long-lived effects were present such as thermally induced changes or photochemical degradation.

The intensity dependent transmission for both samples, in the wavelength range 440–610 nm, shows a clear decrease with increasing input intensity. Fig. 2 shows the intensity-dependent transmission at 580 nm for C_{60} and C_{70}. At high intensity the transmission curve reaches a minimum T_{ex}. The solid line is calculated from the six-level model system as described in the next paragraph. The calculation was made with only one free parameter which was the magnitude of the excited-state absorption cross section.

The interaction of the laser pulse with the C_{60} and C_{70} molecules can be described by a rate equation system. The energy diagram of such a system is shown in fig. 3. Laser pulses excite molecules from the ground state S_0 to the excited Franck–Condon singlet state S_x (absorption cross section σ_g^S). The molecules in this state relax rapidly (≈ 1 ps) into an equilibrium singlet state S_1. This level relaxes either

(a)

(b)

Fig. 2. Transmission versus incident photon flux density at 580 nm, the solid lines are a theoretical calculation based on the six-level model system, the calculation was performed only with the only free parameter C_{60} with $\sigma_{ex} = 7.24 \times 10^{-16}$ and (b) for C_{70} with $\sigma_{ex} = 7.04 \times 10^{-15}$.

to the ground state, with the rate $1/\tau_0$ (ps^{-1}), or to the triplet state with the rate $1/\tau_1$ (ps^{-1}) [13] (intersystem crossing quantum yield 80%) [14]. Excited-state absorption can occur from the singlet state S_1 to higher singlet states S_n (absorption cross section σ_{ex}^S) and from triplet state T_1 to higher triplet states T_n (absorption cross section σ_{ex}^T. Relaxation of these states back to the first excitation states take place very rapidly at the rate of fs^{-1}. The relaxation of the triplet state to the ground state is forbidden and therefore very slow (≈ 100 µs) [14].

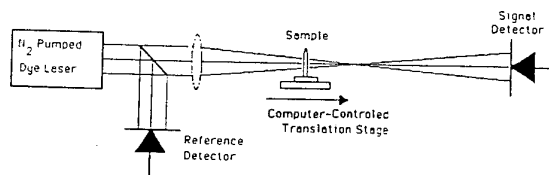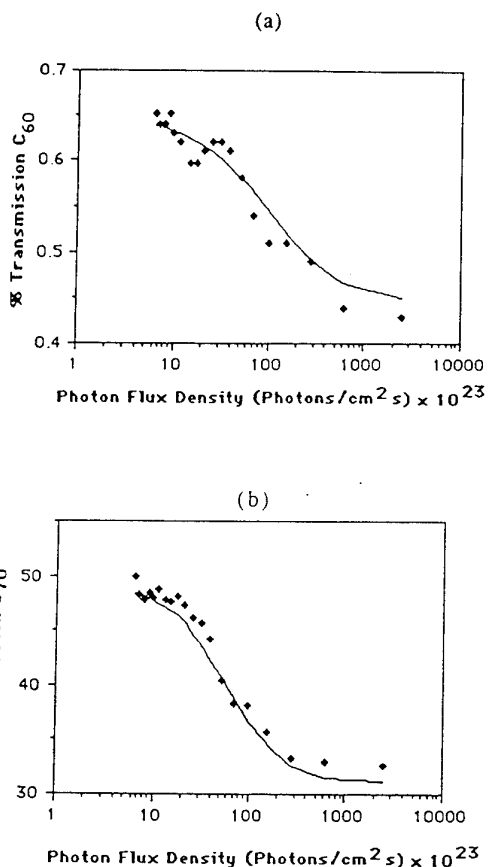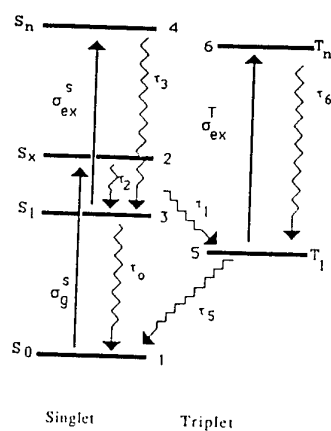The rate equations used to describe the above level system are [15]

Fig. 1. Z-scan experimental apparatus, where transmission is recorded as a function of the position with respect to the focal plane.

145

Singlet   Triplet

Fig. 3. Energy level diagram. The absorption cross sections are given by σ_g^S, σ_{ex}^S and σ_{ex}^T, where g denotes ground state, ex denotes excited state and S, T denoted singlet and triplet states respectively. The life times are given by τ_0, τ_2, τ_3, τ_4, and intersystem crossing by τ_1.

$$\frac{\partial n_1}{\partial t} = \frac{-\sigma_g^S I_L(n_1 - n_2)}{h\nu} + \frac{n_3}{\tau_0} + \frac{n_5}{\tau_5},$$

$$\frac{\partial n_2}{\partial t} = \frac{\sigma_g^S I_L(n_1 - n_2)}{h\nu} - \frac{n_2}{\tau_2},$$

$$\frac{\partial n_3}{\partial t} = \frac{-\sigma_{ex}^S I_L(n_3 - n_4)}{h\nu} + \frac{n_2}{\tau_2} - \frac{n_3}{\tau_0} - \frac{n_3}{\tau_1} + \frac{n_4}{\tau_3},$$

$$\frac{\partial n_4}{\partial t} = \frac{\sigma_{ex}^S I_L(n_3 - n_4)}{h\nu} - \frac{n_4}{\tau_3},$$

$$\frac{\partial n_5}{\partial t} = \frac{-\sigma_{ex}^T I_L(n_5 - n_6)}{h\nu} + \frac{n_3}{\tau_1} - \frac{n_5}{\tau_5} + \frac{n_6}{\tau_6},$$

$$\frac{\partial n_6}{\partial t} = \frac{\sigma_{ex}^T I_L(n_5 - n_6)}{h\nu} - \frac{n_6}{\tau_6},$$

$$\frac{\partial I_L}{\partial Z} = -I_L N[\sigma_g^S(n_1 - n_2) + \sigma_{ex}^S(n_3 - n_4)$$

$$+ \sigma_{ex}^T(n_5 - n_6)], \tag{1}$$

where n_i ($i = 1, ..., 6$) are the population densities of their respective states, τ are the relaxation times, I_L is the laser intensity before entering the sample cell, and t and z represent the normalized temporal and longitudinal coordinates. The first six equations in (1) describe the population changes of the levels by light absorption and relaxation processes. The last equation in (1) describes the change of the laser pulse

146

as it propagates through the sample. Bearing in mind the laser pulse width $T_L = 5$ ns, the following simplifications of the model can be made [16].

(1) Relaxation from the triplet state T_1 to the ground state S_0 will take place on a time scale much longer than the pulse width ($T_L \ll \tau_5$) and thus can be neglected.

(2) The populations of the higher excited states (S_n, T_n) are very small and can be neglected due to their short relaxation times $\ll T_L$.

$$\frac{\partial n_1}{\partial t} = \frac{-\sigma_g^S I_L(n_1 - n_2)}{h\nu} + \frac{n_3}{\tau_0},$$

$$\frac{\partial n_3}{\partial t} = \frac{-\sigma_{ex}^S I_L(n_3 - n_4)}{h\nu} - \frac{n_3}{\tau_0} - \frac{n_3}{\tau_1},$$

$$\frac{\partial n_5}{\partial t} = \frac{-\sigma_{ex}^T I_L(n_5 - n_6)}{h\nu} + \frac{n_3}{\tau_1},$$

$$\frac{\partial I_L}{\partial Z} = -I_L N[\sigma_g^S(n_1 - n_2) + \sigma_{ex}^S(n_3 - n_4)$$

$$+ \sigma_{ex}^T(n_5 - n_6)]. \tag{1a}$$

As the pulse width of the laser is longer than the singlet state lifetime, ($\tau_0 = 600$ ps) and, due to the large quantum yield in this case, the population of this state remains small, the triplet state T_1 acts as an accumulation site. The excitation to the higher states will take place predominantly from the T_1 state (cross section σ_{ex}^T). The level system drawn in fig. 3 is therefore suitable for describing the reverse saturation and for calculating the population density distributions of the different states using the values of the absorption cross sections ($\sigma_{ex}^T > \sigma_g^S$ and $\sigma_{ex}^S > \sigma_g^S$) ($\sigma_{ex}^T \approx \sigma_{ex}^S \approx 8 \times 10^{-16}$ cm^2) and the life times of the excited states. By integrating these equations numerically, the population densities of the various levels can be calculated. An example of these calculations is shown in fig. 4 at intensity $I = 2 \times 10^6$ W/mm^2. From fig. 4 it is clear that with nanosecond pulses the singlet state S_1 level population will remain low compared with that of the triplet state, therefore the excited-state absorption observed, starts from the triplet state ($T_L \gg \tau_0$).

Taking into account the levels involved in the interaction (S_0, S_1, T_1), the above system may be treated effectively as a three-level model where only two absorption cross sections are involved. The
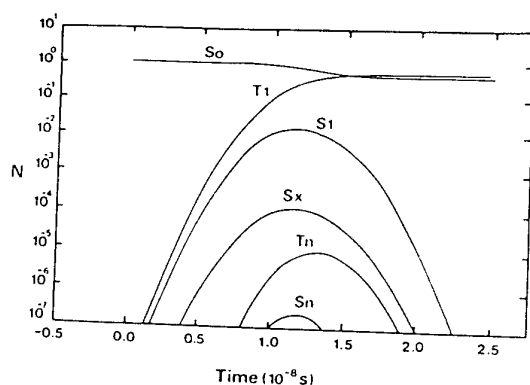
Fig. 4. Calculated population densities N of the levels S_0, T_1, S_x, T_n, S_n. The rate equations for population densities were solved at $I_{max} = 2 \times 10^6$ W/mm^2 and $z = 2$ mm.

change in the absorption coefficient α is related to the saturation intensity which is related to the total absorption α_{tot} for the system,

$$\alpha_{tot} = \sigma_0 n_1 - \sigma_0 n_3 + \sigma_{ex} n_5 ,$$

$$\alpha_{tot} = \frac{\sigma_0 n}{1 + I_L/I_S} + \frac{\sigma_{ex} n}{2 I_S} \frac{I_L}{1 + I_L/I_S} , \qquad (2)$$

here n is the total number density of molecules.

Using the Lambert–Beer law, a saturation transmission is found $T_{sat} = \sqrt{T_0 T_{ex}}$, where T_0 and T_{ex} are the low- and high-level transmissions respectively. The ground- and excited-state absorption cross sections can be calculated from the low- and high-level transmissions and hence give the saturation intensity. The values of these parameters at different values of the wavelengths are given in table 1. In general the rate equation model gives a good fit to the ex-

perimental data and can be used to predict response at a given wavelength from flash photolysis data [13].

The absorption coefficient is directly related to the imaginary part of the third-order nonlinear susceptibility $\mathrm{Im}(\chi^{(3)})$ by

$$\mathrm{Im}(\chi^{(3)}) = \frac{\epsilon_0 c n_0 \lambda \Delta \alpha}{4 \pi I} ,$$

where ϵ_0 is a permitivity of free space, c is the velocity of light, n_0 is the linear refractive index, and λ is a wavelength of the laser, using eq. (2). (For $I \to 0$, $\Delta \alpha = \sigma_0 n$, and at $I = I_{sat}$ $\Delta \alpha = \frac{1}{4} n (\sigma_{ex} - 2\sigma_0)$.) Hence

$$\mathrm{Im}(\chi^{(3)}) = \frac{\epsilon_0 c n_0 \lambda N_A C (\sigma_{ex} - 2\sigma_0)}{16 \pi I_{sat}} , \qquad (3)$$

where N_A is Avogadro's constant and C is a molar concentration.

From the experimental curves, T_{ex} and I_{sat} can be found and then using eq. (3), $\mathrm{Im}(\chi^{(3)})$ can be calculated. Table 1 shows the physical parameter of C_{60} and C_{70}. For a 10^{-5} M solution the values of $\mathrm{Im}(\chi^{(3)})$ are remarkably high.

In conclusion, reverse saturable absorption has been observed for both C_{60} and C_{70} samples and has been explained by a six-level system model. Excited-state absorption cross sections can be estimated and $\mathrm{Im}(\chi^{(3)})$ calculated. Further experiments are being undertaken to study the above effect on fullerene films, where there are considerable problems with photochemical degradation which is not observable in the solution.

Table 1

Calculated parameters of ground-, excited-state absorption cross section σ_0, σ_{ex} and third-order nonlinear susceptibility χ^3

Sample	λ(nm)	σ_0 (cm^2)	σ_{ex} (cm^2)	χ^3 (m^2/V^2)
C_{60}	440	2.96×10^{-16}	8.02×10^{-16}	2.00×10^{-16}
	520	5.2×10^{-16}	1.49×10^{-15}	4.65×10^{-16}
	580	3.5×10^{-16}	7.24×10^{-16}	1.22×10^{-17}
	610	–	–	–
C_{70}	440	–	–	–
	520	5.43×10^{-16}	1.12×10^{-15}	2.48×10^{-17}
	580	4.67×10^{-16}	7.07×10^{-16}	-2.61×10^{-16}
	610	4.52×10^{-16}	5.75×10^{-16}	-6.80×10^{-16}

References

[1] P.N. Butcher and D. Cotter, The elements of nonlinear optics
(Cambridge Univ. Press, Cambridge, 1991).

[2] W. Krätschmer, L.D. Lamb, K. Fostiropoulos and D.R.
Huffman, Nature 347 (1990) 354;
H.W. Kroto, A.W. Allaf and S.P. Blam, Chem. Rev. 91
(1991) 1213; Special Issue on Buckminster-fullerene,
Accounts Chem. Res. 25 (1992) 98.

[3] Y. Achiba, T. Nakagawa, Y. Matusui, S. Suzuki, H.
Shiromaru, K. Yamauchi, K. Nishiyama, M. Kainosho, H.
Hoshi, Y. Maruyama and T. Mitani, Chem. Letters 7 (1991)
1233.

[4] M. Kaiser, J. Reichenbach, H.J. Byrne, J. Anders. W. Maser,
S. Roth, A. Zahab and P. Bentier, Solid State Commun. 81
(1992) 81.

[5] M. Uchida, Y. Ohmori and K. Yoshino, Japan. J. Appl. Phys.
30 (1991) L2104.

[6] W. Blau, H.J. Byrne, D.J. Cardin, T.J. Dennis, J.H. Hare,
H.W. Kroto and R. Taylor, Phys. Rev. Letters 67 (1991)
1423;
Q.H. Gong, Y.X. Sun, Z.J. Xia, Y.H. Zhou, Z.N. Cu. X.H.
Zhou and D. Qiang, J. Appl. Phys. 71 (1992) 3025;

Z.H. Kafafi, J.R. Lindle, R.G.S. Pong, F.J. Bartoli, L.J. Lingg
and J. Milliken, Chem. Phys. Letters 188 (1992) 492.

[7] D.J. Bradley, Ultrashort light pulses, ed. S.L. Shapiro, Topics
Appl. Phys. 18 (1977) 17.

[8] H.J. Eichler, F. Massmann and C.H. Zaki, Opt. Commun.
40 (1982) 302;
K. Bohnert, H. Kalt and C. Klingshirn, Appl. Phys. Letters
43 (1983) 1088.

[9] H.E. Lessing and A. von Jena, Chem. Phys. Letters 59
(1978) 249;
C.R. Guilian and L.D. Hess, IEEE J. Quantum Electron.
QE-3 (1967) 358.

[10] W. Blau, H. Byrn, W.M. Dennis, Opt. Commun. 56 (1985)
25.
L.W. Tutt and S. McGahon, Opt. Letters 15 (1990) 700.

[11] W. Krätschmer, K. Fostiropoulos and D.R. Huffman, Chem.
Phys. Letters 170 (1990) 167.

[12] M. Sheik-Bahae, A.A. Said, T.H. Wei and D.J. Hagan, IEEE
J. Quantum Electron. 26 (1990) 760.

[13] D. Kim, M. Lee. Y.D. Suh and S.K. Kim, Proceeding 8th
International Conference on Ultrafast Phenomena, Antibes,
France, 26-27 (1992).

[14] R.S. Becker, S.M. Hubig, T.J. Dennis, J.P. Hare and H.W.
Kroto, Chem. Phys. Letters, submitted for publication.

[15] H. Stiel, K. Teuchner, D. Leupold, S. Oberländer, J. Ehlert
and R. Jahnke, Intell. Instr. Comp. 9 (1992) 79.

[16] A. Penzkofer and W. Blau, Opt. Quantum Electron. 15
(1983) 325.

ADVANCED MATERIALS

Reprint

Low Power Nonlinear Optical Response of C_{60} and C_{70} Fullerene Solutions**

By *Fryad Z. Henari, Shane MacNamara, Orla Stevenson, Joseph Callaghan, Declan Weldon,* and *Werner J. Blau**

The study of the optical nonlinearity in fullerenes has received considerable attention because of their possible applications in nonlinear optical devices.[1] Similar to organic conjugated polymers and inorganic semiconductors, fullerenes exhibit various types of third-order nonlinear effects, such as third-harmonic generation, two-photon absorption, optical limiting, self-focusing and self-defocusing.[1] The lat-

[*] Prof. W. J. Blau, Dr. F. Z. Henari, S. MacNamara, O. Stevenson,
J. Callaghan
Physics Department, Trinity College, University of Dublin
Dublin 2 (Ireland)
D. Weldon
Chemistry Department, Trinity College, University of Dublin
Dublin 2 (Ireland)

ter properties are based on an intensity-dependent refractive index. The laser light induces a localized change in refractive index that results in a lensing effect on the beam at a certain threshold value of intensity. A positive refractive index change causes self-focusing, whereas a negative refractive change results in self-defocusing. This can be used to obtain a quantitative measurement of the third-order nonlinear susceptibility, χ^3, using the Z-scan techniques[2] described below.

In most nonlinear optical experiments, high peak power and short pulse duration are required in order to induce a measurable effect. With picosecond laser pulses, ultrafast off-resonant third-order nonlinearities of up to 10^{-34} esu per molecule[3] have been reported in fullerenes. When the laser is tuned to a frequency within the electronic absorption bands of the material, a resonant enhancement of the nonlinearity by several orders of magnitude is observed. In fullerenes, this manifests itself as an intensity-dependent absorption, leading to efficient optical limiting behavior via the saturation of the molecule's lowest triplet state.[4] As the relaxation time of the triplet state is generally slow (in the range of 100 µs in fullerenes[5]), it should be possible to observe nonlinear behavior with low-power laser irradiation.[6] Under continuous wave irradiation, however, there is usually an additional, large, thermally induced nonlinearity in common organic materials (such as dye solutions or conjugated polymers), which dominates all other electronic processes. This thermal effect arises from the predominantly non-radiative relaxation of the excited states, which causes a local temperature rise and thus a refractive index change through the thermo-optic coefficient, dn/dT. Despite being a slow (microseconds to milliseconds decay time) process, the thermally induced refractive index change has a considerable number of potential applications in the fields of thermal calorimetry[7] and optical bistability.[8]

In the following, we report measurements of the third-order nonlinear optical response of C_{60} and C_{-0} in solution with continuous wave (cw), low-power visible lasers. We discuss the origin of the observed nonlinearity, which, we believe, results from a combination of thermal effect and triplet state saturation that is unique to fullerenes.

The C_{60} and C_{70} samples were prepared by contact-arc evaporation of graphite in a helium gas atmosphere.[9] followed by extraction of the soot with CS_2 and chromatographic purification in an oxygen-free N_2 atmosphere. The samples have a purity of 99.99% and can be dissolved in degassed benzene or toluene. The concentrations of C_{60} and C_{70} were chosen to be 10^{-3} M (in benzene) and 10^{-5} M (in toluene), respectively. The linear absorption of the solutions agrees with values published elsewhere.[10]

The experimental technique used in these measurements is very similar to that described by Sheik Bahae et al.[2] (Z-scan technique) and is shown in Figure 1. Briefly, the technique relies on the fact that intensity varies along the axis of a convex lens and is maximum in the focus. Hence, by shifting a thin sample through the focus, the intensity-dependent
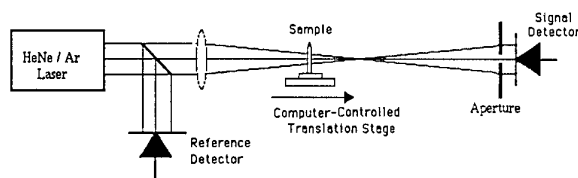

Fig. 1. Z-scan experimental set-up, where transmission is recorded as a function of the position with respect to the focal plane.

absorption can be measured as a change of transmission. The nonlinear refraction is determined by the spot size variation at the plane of a finite-aperture detector combination because the sample itself acts effectively as a thin lens with varying focal length as it traverses the focal plane. The experiments were performed with low power cw lasers, specifically a HeNe laser (wavelength $\lambda = 632.8$ nm) and an air cooled Ar laser operating on either the 514 nm or the 488 nm line. The average powers of both lasers were adjusted to be 15 mW. The laser beam was chopped at frequencies ranging from 50 to 400 Hz. It was focused to a beam waist of $w_0 = 48$ µm with a lens of 6 cm focal length, giving a typical power density of 10^6 W m^{-2}. Each data point plotted corresponds to an average of 15 independent measurements.

The transmission for the samples was simultaneously measured with and without an aperture in the far-field of the lens, as the sample moved through the focal point. This enables the nonlinear refractive index (closed aperture) to be separated from that of the nonlinear absorption (open aperture). Generally, the variation of the complex refractive index Δn with intensity I can be taken as linear, where the real part $\mathrm{Re}\{\Delta n\} = \gamma I$ corresponds to the refractive index change and the imaginary part $\mathrm{Im}\{\Delta n\} = \beta I$ refers to the nonlinear absorption. Figure 2 shows the normalized transmittance without an aperture as a function of the distance along the lens axis, z, for a 1 mm thick cuvette of C_{60} solution at $\lambda = 488$ nm. This measurement corresponds to the open aperture condition and the decrease of absorption with in-
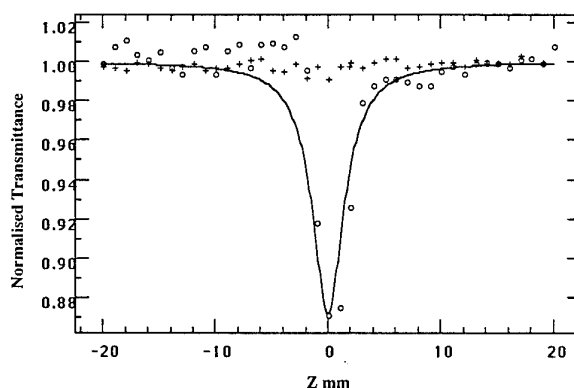

Fig. 2. Normalized transmittance (open aperture) at 488 nm of C_{60} (o) and of the solvent, toluene (+). The solid line is a fit of the data to Equation 1 with $\beta = 12$ m/MW.

tensity indicates a nonlinear absorption (sometimes also termed reverse saturable absorption). In order to establish that the effect seen is due to C_{60}, the Z-scan (open aperture) was performed also with just the pure solvent. In this case, no nonlinear absorption was observed within the limit of the intensity used in the experiment (see Fig. 2). We conclude that the effect seen is totally due to fullerene.

The normalized transmittance for the open aperture condition is given by Equation 1.[2]

$$T(z) = \sum_{m=0}^{\infty} \frac{(-q_0)^m}{(m+1)^{3/2}} \quad \text{for} \quad |q_0| < 1 \tag{1}$$

where

$$q_0 = \frac{\beta I_0 (1 - e^{-\alpha L})}{(1 + z^2/z_0^2)\alpha}$$

Here, α is the absorption coefficient in m^{-1}, L is the thickness of the sample, I_0 is the intensity of the laser beam at the focus ($z = 0$), and z_0 is the Rayleigh range of the lens. A fit of Equation 1 to the experimental data is depicted in Figure 2 and yields a value of $\beta = 12 \pm 4$ m/MW for the nonlinear absorption. The decrease of the transmittance with the intensity is indicative of optical limiting and has been observed by various authors with different pulsed lasers.[1, 4] The value of $\beta = 12$ m/MW should be compared to the value of $\beta = 0.05$ m/GW[2] observed in C_{60} films, indicating a more favorable condition for two-photon absorption in the dilute solution, probably due to a longer lifetime ($\tau_T = 0.1$ ms) of the triplet T_1 state in solution. Two-photon absorption in this case proceeds as a two-step excitation process via a real intermediate triplet state. The lifetime of this state therefore affects the apparent two-photon absorption coefficient.

The normalized transmittance through a closed aperture at wavelength $\lambda = 632$ nm is shown in Figure 3. The peak–valley configuration of this Z-scan is indicative of a negative (self-defocusing) nonlinearity. Self-defocusing in both C_{60}

Fig. 4. A series of photographs showing the variation of the spot size as a function of sample position relative to the lens focus. a) Before focus, no nonlinear effects present; b) prefocal transmittance maximum; c) at focus; d) postfocal transmittance minimum; e) after focus, no nonlinear effects present.
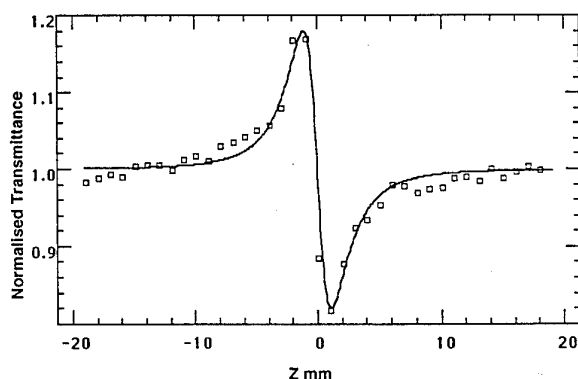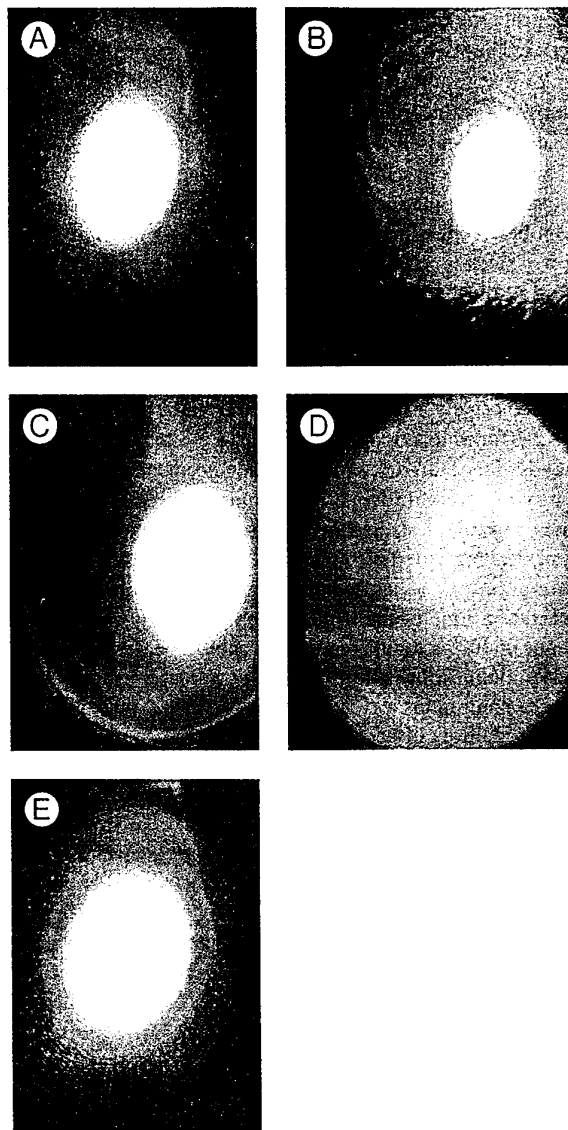

Fig. 3. Normalized transmittance (closed aperture) of C_{60} at 632 nm. The solid line is a fit of the data to Equation 2 with $\Delta\phi = 0.887$ and aperture size $S = 0.1$.

and C_{70} solutions was also observed with the naked eye. Figure 4 shows the variation of the spot size as a function of sample position relative to the focal plane at $\lambda = 514$ nm. The first photograph was taken well before focus $(-z)$, where the nonlinear effects are negligible. The second was taken at the prefocal aperture transmittance peak (see Fig. 3), the third at the focus, the fourth at the postfocal transmittance minimum, and the fifth well after focus $(+z)$ where the nonlinear effects are also negligible.

The normalized transmission for the closed aperture Z-scan is given by Equation 2,[2] where $P_i(t) = \pi w_0^2 I(t)\ 2$ is the

instantaneous input power and S is the aperture's linear transmission.

$$T(z) = \frac{\int P_{\mathrm{f}}(\Delta\phi(t))\,\mathrm{d}t}{S\int P_{\mathrm{i}}(t)\,\mathrm{d}_t} \qquad (2)$$

The solid line in Figure 3 is obtained by fitting the above equation using $\Delta\phi = -0.887$. Values of $\Delta\phi$. the phase variation, are calculated from the peak–valley transmission difference $\Delta T_{\mathrm{p-v}} = 0.406\,(1-S)^{0.25}|\Delta\phi|$.

The nonlinear index γ is given by Equation 3.[2] and the real part of the third-order nonlinear susceptibility $\chi^{(3)}$ is related to γ through Equation 4.

$$\gamma = \frac{\Delta\phi(t)\lambda\alpha}{2\pi I_0(1-\mathrm{e}^{-\alpha L})} \qquad (3)$$

$$\mathrm{Re}\{\chi^{(3)}\} = 2n^2\varepsilon_0 c\gamma \qquad (4)$$

Here n is the linear refractive index, ε_0 is the permittivity of free space and c is the velocity of light. The experimentally determined values of $\mathrm{Re}\{\chi^{(3)}\}$ ($\pm 12\%$) for different wavelengths are given in Table 1. They are in the range of 10^{-14}–

Table 1. Nonlinear susceptibilities and other experimentally determined parameters for C_{60} and C_{70} solutions.

Sample	λ [nm]	$\mathrm{Re}\{\chi^{(3)}_{\mathrm{exp.}}\}$ [m^{2}V^{-2}]	$\chi^{(3)}_{\mathrm{therm}}$ [m^{2}V^{-2}]	$\Delta\phi$	α [m^{-1}]
C_{60}	632	-3.20×10^{-14}	-7.25×10^{-14}	0.887	124
	514	-3.71×10^{-14}	-1.88×10^{-13}	0.648	336
	488	-2.08×10^{-13}	-1.44×10^{-13}	0.628	247
C_{70}	632	-4.69×10^{-14}	-9.28×10^{-14}	0.773	223
	514	-2.47×10^{-14}	-1.12×10^{-13}	0.538	298
	488	-1.19×10^{-14}	-6.44×10^{-12}	0.568	164

10^{-13} m^{2}V^{-2} (10^{-6}–10^{-5} esu), which is large for organic materials. The normalized transmittance through a closed aperture at $\lambda = 632$ nm for different concentrations and for pure solvent is shown in Figure 5, left. The peak–valley variation for different concentrations indicates that the effect is due to the fullerene. The third-order nonlinear susceptibility $\chi^{(3)}$ can be related to the molecular hyperpolarizability γ through $\chi^{(3)} = L^4 C N_{\mathrm{A}}\gamma$. where $L^4 = (n^2+2)/3$ is the Lorentz local field factor, C the concentration. N_{A} Avogadro's constant, and n the refractive index. The $\chi^{(3)}$ in C_{60} is concentration dependent, which can be confirmed experimentally. see Figure 5, right.

For an electronically resonant third-order nonlinearity we expect several contributions to $\mathrm{Re}\{\chi^{(3)}\}$:[10]

– resonant optical Kerr effect,
– thermally induced refractive index changes.
– absorption saturation.

Of these, the first can be excluded due to its size (generally, $\mathrm{Re}\{\chi^{(3)}\} <10^{-10}$ esu) and time scale (generally, relaxation time $\tau <10^{-9}$ s).[10] The absorption contribution to $\mathrm{Re}\{\chi^{(3)}\}$ is from two-photon absorption, where the Kramers–Kronig
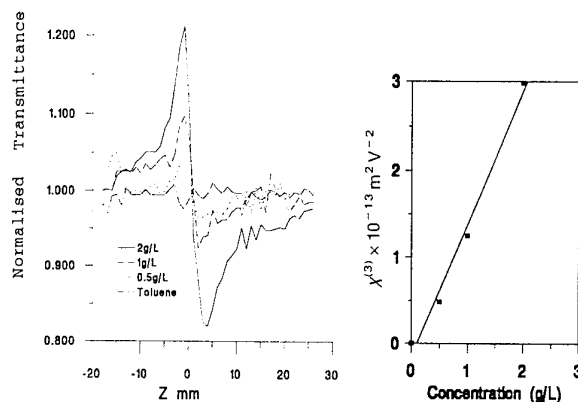

Fig. 5. Left) Normalized transmittance (closed aperture) of C_{60} at 623 nm at different concentrations and of the solvent. toluene. Right) Nonlinear susceptibility $\chi^{(3)}$ of C_{60} versus concentration.

relation states that the change in refractive index at any frequency is associated with a change of absorption coefficient.

The theoretical description of the thermally induced refractive index change is well established[11] and given by Equation 5, where $\Delta n_0 = \gamma I_0$ from Equation 3. The corresponding real third-order nonlinear susceptibility $\chi^{(3)}_{\mathrm{therm}}$ is given by Equation 6.

$$\Delta n_0 = -\left(\frac{\mathrm{d}n}{\mathrm{d}T}\right)\frac{F_0\alpha}{2\rho C_{\mathrm{p}}} \qquad (5)$$

$$\chi^{(3)}_{\mathrm{therm}} = -\frac{\mathrm{d}n}{\mathrm{d}t}\frac{\alpha n_0^2\varepsilon_0 c F_0}{\rho c_{\mathrm{p}} I_0} \qquad (6)$$

In these equations. $\mathrm{d}n/\mathrm{d}t$ is the change of refractive index with temperature (thermo-optic coefficient). F_0 is the laser fluence. ρ is the density, and c_{p} is the specific heat. The rise time of the thermally induced lens in the liquid is determined by the acoustic transit time, $\tau_{\mathrm{r}} = w_0/v$, and the decay time $\tau_{\mathrm{d}} = \rho(c_{\mathrm{p}}/K)w_0$, where w_0 is the beam waist. v is the velocity of sound in the liquid, and K is the thermal conductivity. For benzene $v = 1296$ ms^{-1}, and with the beam waist $w_0 = 48$ µm. the rise and decay times are 37 ns and 28 ms. respectively. Therefore we can regard the heating caused by the chopped laser at frequencies up to 400 Hz as quasi steady state. The values of $\chi^{(3)}_{\mathrm{therm}}$ were calculated using the thermal parameters listed in Table 2 for the solvents used in the experiments. and are given in Table 1.

A comparison between the experimental $\mathrm{Re}\{\chi^{(3)}\}$ values and the calculated thermal $\chi^{(3)}_{\mathrm{therm}}$ values suggests that one major contribution to the nonlinear response is indeed of thermal origin, especially as the measured values all have a negative sign. It should be noted, however, that Equation 6 predicts a linear relationship between $\chi^{(3)}_{\mathrm{therm}} I_0$ and the absorption coefficient α. This is not verified experimentally and indicates that absorption saturation must also be considered.

Table 2. Relevant thermal data for the calculation of thermally induced refractive index changes.

	Units	Benzene	Toluene
n		1.5	1.49
c_p	$J kg^{-1} K^{-1}$	1.72	1.67
k	$W m^{-1} K^{-1}$	0.421	0.135
dn/dt	K^{-1}	-6.8×10^{-4}	-4.2×10^{-4}
ρ	$kg m^{-3}$	950	943

A theoretical description of the optical nonlinearity originating from the saturation of the ground state absorption in a four-level system similar to the one used for the description of optical limiting in fullerenes[4] was given by Steel et al.[12] Intensity-dependent absorption can be observed if the ground-state absorption (which is rather weak in fullerenes in the visible because the optical transitions there are in principle forbidden) is smaller than the excited-state absorption. The triplet state T_1 acts as a metastable accumulation site with a rather long lifetime, $\tau \sim 0.1$ ms,[5] giving an exceptionally low ground state saturation intensity of $I_s = 10^3$ to 10^4 $W cm^{-2}$. This is in agreement with the magnitude of the nonlinear absorption coefficient β reported above. Inserting these values into the lengthy equations given by Steel et al.[12] yields values for the nonlinear susceptibility due to absorption saturation in the range of $\chi_{sat}^{(3)} = 10^{-14}$ to 10^{-13} $m^2 V^{-2}$. This is of the right order of magnitude to account for the difference between the experimentally measured values and the calculated thermal contribution. A direct comparison of experimental and calculated values should be treated cautiously in any case because the calculation requires a precise knowledge of position, line shapes, and line broadening mechanisms of the electronic states.

In conclusion, a remarkably large low-power third-order nonlinearity at different visible wavelengths has been measured in C_{60} and C_{70} solutions. The negative sign of the nonlinear refractive index data is indicative of the dominance of the thermo-optic effect. The special electronic structure of fullerenes, however, is responsible for a further contribution due to reverse saturable absorption. The use of laser beams chopped at frequencies up to 400 Hz demonstrates that the nonlinearity is faster that 2.5 ms. Nonlinearities of this kind may be useful in various all-optical devices[1,8] if the fullerenes are dispersed in a transparent polymer matrix (rather than in solution), where the polymer matrix preserves the same properties as in solution.[13] An experiment on using these materials as an on–off switch is in progress.

[1] For a brief review, see W. J. Blau, D. J. Cardin, *Mod. Phys. Lett. B* **1992**. 6, 1351.
[2] M. Sheik Bahae, A. A. Said, T. H. Wei, D. J. Hagan, E. W. Van Stryland. *IEEE J. Quantum Electron.* **1990**, 26, 760.
[3] W. J. Blau, H. J. Byrne, D. J. Cardin, *Phys. Rev. Lett.* **1991**, 67. 1423.
[4] L. W. Tutt, A. Kost, *Nature* **1992**, 356, 225. F. Z. Henari, J. Callaghan, H. Stiel, W. Blau, D. J. Cardin, *Chem. Phys. Lett.* **1992**, 199, 144.
[5] J. W. Arbogast, A. P. Darmanyan, C. S. Foote, Y. Rubin, F. N. Diederich, M. M. Alvarez, S. J. Anz, R. L. Whetten, *J. Phys. Chem.* **1991**. 95, 11.
[6] S.-C. Yang, Q. Gong, Z. Xia, Y. H. Zhou, Y. Q. Wu, D. Qiang, Y. L. Sun. Z. N. Gu, unpublished.
[7] J. M. Harris, N. J. Dovichi, *Anal. Chem.* **1980**. 52, 695 A.
[8] W. Blau, *Opt. Commun.* **1987**, 64, 85.
[9] W. Krätschmer, L. D. Lamb, K. Fostiropoulos, D. R. Huffman. *Nature* **1990**, 347, 354.
[10] H. W. Kroto, A. W. Allaf, S. P. Blam, *Chem. Rev.* **1991**, 91, 1213. See also Special Issue on Buckminsterfullerene. *Acc. Chem. Res.* **1992**. 25, 98.
[11] J. N. Hayes. *Appl. Opt.* **1972**, 2, 455.
[12] D. R. Steel, R. C. Lind, J. F. Lam, *Phys. Rev. A* **1981**, 23, 2513.
[13] A. Kost, L. Tutt, M. Klein, T. Gougherty, W. Elias. *Opt. Lett.* **1993**. 18, 334.

H. Kuzmany   J. Fink   M. Mehring   S. Roth (Eds.)

Electronic Properties of Fullerenes

Proceedings of the International Winterschool on
Electronic Properties of Novel Materials,
Kirchberg, Tirol, March 6–13, 1993

With 238 Figures

Linear and Nonlinear Optical Properties of Fullerenes and Some Metal Derivatives

J. Callaghan[1], D.N. Weldon[2], F.Z. Henari[1], W. Blau[1], and D.J. Cardin[3]

[1]Department of Pure and Applied Physics, Trinity College, Dublin 2, Ireland
[2]Department of Chemistry, Trinity College, Dublin 2, Ireland
[3]Department of Chemistry, University of Reading, Reading RG11 6AD, UK

Abstract. Fullerene C_{60} and C_{70} have been prepared using the contact arc method, purified and used to synthesise metal derivatives with the metals iridium (Ir), platinum (Pt), and palladium (Pd). Non-linear optical studies of these materials in the sub nanosecond regime have been carried out employing the technique of Saturation Spectroscopy permitting the magnitudes of the imaginary component of the third order non-linear susceptibility to be obtained.

1. Introduction

The non-linear optical properties of fullerenes have been likened to those of conjugated organic polymers, where the behaviour is attributed to extensive π electron delocalization, resulting in a highly polarizable material. Recently Tutt and Kost [1] have reported optical limiting in solutions of C_{60} as have also Henari et al. [2]. This behaviour has been explained in terms of excited state absorption, and has been observed in a number of materials including semiconductors [3], dyes and organometallic materials [4].

Here we report the synthesis of metal derivatives of C_{60} and C_{70} and a comparative study of their intensity dependant absorption with their parent molecule. The metals used were the transition metals iridium (Ir), platinum (Pt), and palladium (Pd), each metal being co-ordinated with two carbon atoms of the fullerene cage.

2. Synthesis of (η^2-$C_{60/70}$M) Derivatives and Experimental Proceedure.

Fullerenes were prepared in the usual manner using the contact arc method [5]. For a typical preparation of the fullerene derivatives, 3.10^{-5} moles of C_{60} or C_{70} powder was dissolved in 25ml of dry degassed toluene. The metal reactants were dissolved in a similar amount of dry degassed toluene and added dropwise over ten minutes to a stirring solution of the fullerene using a cannula. Work-up of the products involved removal of the toluene on a vacuum line followed by washing the product in a Schlenk tube with dry degassed ethanol. The powders were then dried on a vacuum line for 2 hours. All manipulations of the products were carried out in a Millar-Howe drybox with O_2 and N_2 levels of less than 1ppm. The products were
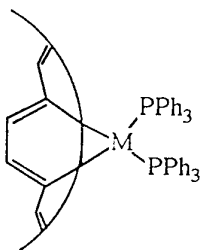
η²-coordination in
metallofullerenes

Fig. 1 Structural representation
of C_{60}/C_{70} metal derivative.
M=Ir, Pd, or Pt

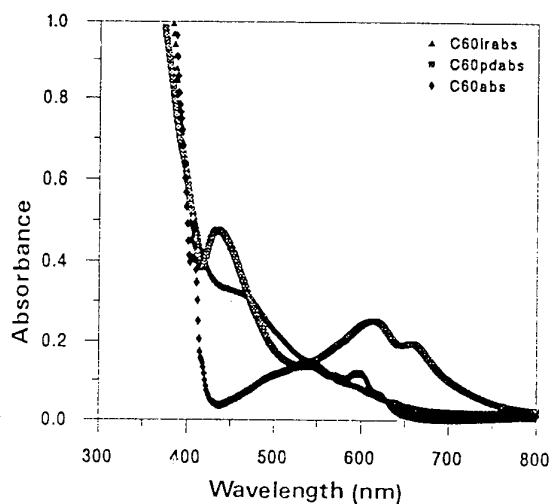Fig. 2 Absorption spectra of C_{60}, $C_{60}Pd$
and $C_{60}Ir$

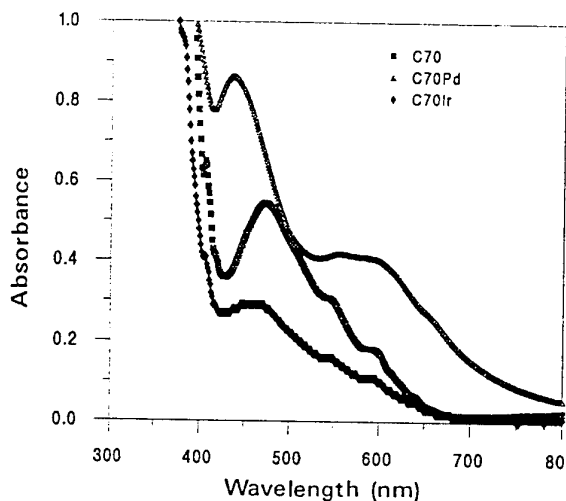Fig. 3 Absorption spectra
of C_{70}, $C_{70}Pd$ and $C_{70}Ir$

Fig. 4 Plot

pulsewidth
40μJ/pulse.
and placed
through the
incident int(
oscilloscope
The maxi
points were
transmissioi
$C_{60}Ir$ and C

3. Results a

Addition of
compared tc
750nm, 100
from Fig.2,
palladium a
450nm, but

analysed and structures assigned using a combination of IR, UV/VIS/NIR, NMR
and FABMS. Fig.1 shows a schematic representation of η^2- bonding to the metal.

Solutions of the metal derivatives were made up in dry degassed toluene. each
with a concentration of 2g/L. The absorption spectra for C_{60}, $C_{60}Ir$, $C_{60}Pd$, and
the corresponding derivatives of C_{70} are shown in Figs 2 and 3, respectively.

The non-linear absorption experiments were performed using a PRA LN100
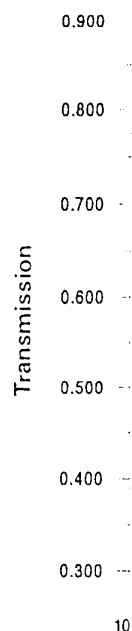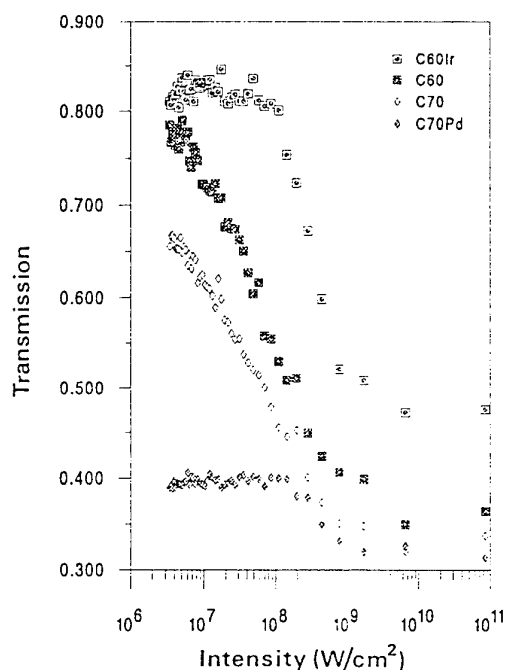Nitrogen pumped dye laser with Rhodamine 6G as the lasing dye. This laser has a

308

Fig. 4 Plot of intensity dependant transmission for C_{60}, C_{70} C_{60}Ir and C_{70}Pd

pulsewidth of 500ps and lasing at 588nm gave a typical energy output of 40μJ/pulse. Samples under investigation were contained in 1mm quartz cuvettes and placed on a linear translation stage. This permits the sample to be moved through the focal plane of a 5cm lens. Variations in the transmitted fluence with incident intensity are monitored using wide area photodiodes, and a digital storage oscilloscope interfaced to a PC.

The maximum incident intensity was 100GW/cm^2, occurring at focus. Data points were averaged over 20 laser shots with a repetition rate of 1Hz. A plot of the transmission as a function of incident intensity is shown in Fig. 4 for C_{60}, C_{70}, C_{60}Ir and C_{70}Pd.

3. Results and Discussion

Addition of the metal sidegroups has greatly changed the absorption spectra compared to those of C_{60} and C_{70}. In the case of C_{60}Pd the λ_{max} is now around 750nm, 100nm further in the red than that of C_{60}. Also, though it cannot be seen from Fig.2, the large C_{60} peak at 350nm has been shifted well below 300nm. The palladium and platinum (not shown) derivatives both have a sharp peak near 450nm, but in the iridium compound this is absent. Indeed the visible section of the

309

Table 1 List of calculated absorption cross sections and $\chi^{(3)}$ for C60, C70 and their metal derivatives

Compound	σ_0 (cm^2)	σ_{ex}/σ_0	$\chi^{(3)}$ (m2/V2)
C60	$1.45 . 10^{-18}$	4.16	$1.78 . 10^{-16}$
(η^2-C60)Pd(PPh3)2	$5.61 . 10^{-18}$	1.62	$1.55 . 10^{-17}$
(η^2-C60)Pt(PPh3)2	$1.14 . 10^{-17}$	1.44	$1.32 . 10^{-16}$
(η^2-C60)IrCOI(PPh2Me)2	$2.56 . 10^{-18}$	2.78	$4.14 . 10^{-17}$
C70	$2.94 . 10^{-18}$	2.74	$7.55 . 10^{-17}$
(η^2-C70)Pd(PPh3)2	$1.16 . 10^{-17}$	1.22	$5.78 . 10^{-17}$
(η^2-C70)IrCOI(PPh2Me)2	$3.46 . 10^{-18}$	2.58	$2.64 . 10^{-17}$

iridium absorption spectra has no distinguishing features, being characterised solely by a gradual increase in the absorption from 700nm down to 350nm with small very weak transitions observable near 600nm, 550nm and 475nm

The palladium and platinum derivatives of C70 show qualitatively the same behaviour as those of C60. We see absorption starting at 800nm for C70Pd and the large peaks at 350nm and 480nm being shifted into the blue. For the C70Ir species the same blueshift is observed but the λ_{max} remains the same as that of C70.

C60 has been shown to possess a long lived first excited triplet state with a lifetime between 40μs [6] and 400μs [7]. Initial excitation of the molecule results in populating the excited singlet levels S_1, S_2,...S_n. These rapidly relax to the first excited singlet and, via a fast intersystem crossing, populate the first excited triplet. This level thus acts as an accumulation site from which excited state absorption may result. Thus to a large extent there are two levels involved in any excitation process, as the population of the S_1 state is much smaller than that of S_0 or T_1. For a two level system the following equation may be derived for the change in absorption ($\Delta\alpha$), in terms of the saturation intensity I_{sat} and the ground and excited state absorption cross sections (σ_g,σ_{ex}) [2].

$$Im(\chi(3)) = \frac{\varepsilon_0 cn\lambda N_A C(\sigma_a - \sigma_0)}{16\pi I_{sat}}$$

where N_A is Avogadro's constant, n the linear refractive index, λ the laser wavelength and C the molar concentration (Table 1).

For the fu
of the parc
limiting bo
conjugation
brought abc
metal sideg
In conclu
limiting bel
the same ra
the authors
their Im $\chi^{(3)}$
real compor

References

[1] L. W. Tu
[2] F. Z. Her
Lett 199 (19
[3] H. J. Eic
[4] W. Blau,
[5] W.Kratsc
[6] J. W. Arl
M. Alvarez,
[7] M. R. W:
J. Am. Chen

For the fullerene derivatives we see that the Im $\chi^{(3)}$ values are smaller than those of the parent C_{60} or C_{70}. and consequently show a smaller degree of optical limiting behaviour. This may be explained in terms of a reduction of the conjugation in the molecule and a decrease in the level of electron delocalization, brought about by the bonding of two of the carbon atoms in the fullerene cage to the metal sidegroup, but differences in the photodynamics may also contribute to this.

In conclusion new metal derivatives of fullerenes have been prepared and optical limiting behaviour observed in them. This phenomenon has been analysed using the same rate model that has been shown to be relevant to the parent fullerenes (but the authors acknowledge that this may not be entirely valid) and the magnitudes of their Im $\chi^{(3)}$ calculated. Further experiments are underway to obtain the size of the real component and will be reported shortly.

References

[1] L. W. Tutt and A. Kost, Nature. 356 (1992) 225

[2] F. Z. Henari, J. Callaghan. H. Stiel. W. Blau and D. J. Cardin, Chem. Phys. Lett 199 (1992) 144.

[3] H. J. Eichler, F. Massmann and C. H. Zaki, Opt. Commun. 40 (1982) 302

[4] W. Blau, H. Byrne, W. M. Dennis. J. M. Kelly, Opt. Commun. 56 (1985) 25

[5] W.Kratschmer, L. D. Lamb, K. Fostiropoulos and D. R. Huffman, Nature 347

[6] J. W. Arbogast, A. P. Darmanyan. C.S. Foote, Y. Rubin, F. N. Diederich, M. M. Alvarez, S. J. Anz and R. L. Whetten. J. Phys. Chem. 95 (1991) 11.

[7] M. R. Wasielewski, M. P. O'Neill. K.R. Lykke, M. J. Pelin and D. M. Gruen, J. Am. Chem. Soc. 113 (1991) 2774

H. Kuzmany J. Fink M. Mehring S. Roth (Eds.)

Electronic Properties of Fullerenes

Proceedings of the International Winterschool on
Electronic Properties of Novel Materials,
Kirchberg, Tirol, March 6–13, 1993

With 238 Figures

Characterisation of Fullerene Schottky Diodes

S. Curran[1], J. Callaghan[1], D. Weldon[2], E. Bourdin[1], K. Cazini[1], W.J. Blau[1], E. Waldron[3], D. McGoveran[1], M. Delamesiere[2], Y. Sarazin[1], and C. Hogrel[1]

[1]Department of Pure and Applied Physics, Trinity College Dublin, Dublin 2, Ireland
[2]Chemistry Department, Trinity College Dublin, Dublin 2, Ireland
[3]Microelectronics and Electrical Engineering Department, Trinity College Dublin, Dublin 2, Ireland

Abstract.

The fabrication and characterisation of the fullerenes C_{60} and C_{70} as semiconductors in Schottky diodes are reported. The preparation of these devices involved forming a Schottky barrier between heavily doped n-Si and Ca with C_{70}, and Mg-In with C_{60}. Electrical diode characteristics are determined and from these measurements both the device quality and the electron affinity of C_{60} and C_{70} were calculated. The value obtained for the electron affinity of C_{60} is in good agreement with other work reported in this area. In the case of n-Si/C_{70} Schottky diode the efficiency as a photovoltaic device was also investigated.

1 Introduction

Since the discovery of this new class of materials the fullerenes have been investigated in great detail towards practical technological application. Studies have ranged from electronic devices such as MIS[1] and FET[2] to the area of superconductors[3]. The following is a report for their application as Schottky diodes.
A Schottky diode is a device which is formed when a metal and a semiconductor come into contact. These diodes are normally majority carriers except on rare occasions when a drift current is introduced. The materials used for these devices are:

1) Au/C_{70}/n-Si,
2) ITO/C_{70}/Ca/Al,
3) ITO/C_{60}/Mg-In.

The Schottky diode formed is between the fullerene and the low work function materials: n-Si, Ca, Mg-In, where the work functions vary between 2.5 - 3.9 eV. From these measurements it is possible to obtain the diode quality factor and the electron affinity value.

427

2 Schottky Diode Theory

When a metal makes contact with a semiconductor the fermi levels of the two materials must be coincident at thermal equilibrium. The equilibrium charge distribution is in the region of the metal/semiconductor interface. For n-type diode characteristics the Schottky diode is similar to that of a one sided abrupt p-n junction. Unlike their counterparts the p-n junction diodes of the Schottky diode is dependent on majority carriers for current transport. There are a number of methods of analysing the current characteristics of the diodes.

1) Thermionic Emission: This theory is based on the assumption that the barrier height $q\Phi_{Bn}$ is much larger than kT, and thus is highly temperature dependent.
2) Isothermal Diffusion: This theory neglects the effect of temperature and is dependent on electron collisions within the depletion region as well as the fact that the carrier concentration within the depletion region is unaffected by the current flow (i.e. they are in equilibrium).
3) Drift Carrier Transport: In this case the minority carriers dominate the transport mechanism in the device.

The barrier height between metal and semiconductor is given by:

$$q\Phi Bn = q(\Phi_m - \chi),$$

where Φ_m is the metal work function and χ is the electron affinity value. The general expression which incorporates all these theories can be described as follows:

$$Jn = Jsat \exp\frac{qV}{kT} - 1 \ .$$

V is the applied voltage and J_{sat}, the saturation current, can be described by:

$$Jsat = A * T^2 \exp\frac{-q\Phi Bn}{kT}$$

The above expression is a generalised form of the saturation current for the three theories, where A^* is the Richardson's constant for thermionic emission into a vacuum ($A^* = 120$ mA/cm^2/K) and Φ_{Bn} is the barrier height. The barrier height, and hence the electron affinity can be obtained as follows:

$$\Phi Bn = \frac{kT}{q} Ln(\frac{A * T^2}{Jsat})$$

428

The effec
large for
(the rati
current)
becomes
concentrat
conductior
whether on

3 Device

Evaporatio
2×10^{-6} mba
two hours.
200 nm. Th
at a press
minutes an
obtain an
sputtering
The follow

Area of Mg
Area of n-
Area of Al

4 Analysi

It can be
good charac
diodes[4].
2 to 2.75 v
overall are
response of
similar. Wh
obvious cho
low work f
Fig.1 is th
possible to
work functi
possible to
However, th
to the allo
weaker the
electron aff
to date us
metal conta
calcium (di
result of u
affinity is
stable as ot

The effect of the minority carriers must be analysed. At large forward bias the minority carrier injection ratio γ (the ratio of minority carrier current to the total current) increases due to the drift field component which becomes larger than the diffusion current. The concentration of the number of carriers available for the conduction process plays a large part in dictating whether or not which process will dominate.

3 Device Preparation

Evaporation of C_{60} and C_{70} was performed at a pressure of 2×10^{-6} mbar in the temperature range of 690K to 750K for two hours. This procedure resulted in a film thickness of 200 nm. The metals Ca, Mg-In and Al were all evaporated at a pressure of 2×10^{-6} mbar. This procedure took five minutes and resulted in a metal thickness of 500 nm. To obtain an Au layer a sputtering device was used. The sputtering lasted 30s and gave a film thickness of 200 A°. The following are the areas of the diodes:

Area of Mg-In/C_{60}/ITO: 4mm,
Area of n-Si/C_{70}/Au: 3.8cm,
Area of Al/Ca/C_{70}/ITO: 4.2cm.

4 Analysis

It can be seen clearly that all three diodes show quite good characteristics not dissimilar to most other organic diodes[4]. The exponential expansion is in the region of 2 to 2.75 volts, depending on the size of the device. The overall area difference is not that great so that the response of all three would be expected to be somewhat similar. When considering electrode materials, the most obvious choice are those incorporating very high and very low work functions. The diode characteristics shown in Fig.1 is the Mg-In/C_{60} device. By using Mg-In alloy it was possible to produce a stable electrode contact with a low work function. From the diode characteristics it was thus possible to derive the C_{60} electron affinity value. However, this value is larger than expected probably due to the alloy used. The higher the work function used the weaker the Schottky effect and thus the exactness of the electron affinity value. The most common diode fabricated to date using organic materials[5] is one which has metal contacts consisting of ITO (Indium Tin Oxide) and calcium (diode characteristics are shown in Fig.2). The result of using these is that the value of the electron affinity is quite good. However, this device is not as stable as others that may be used.
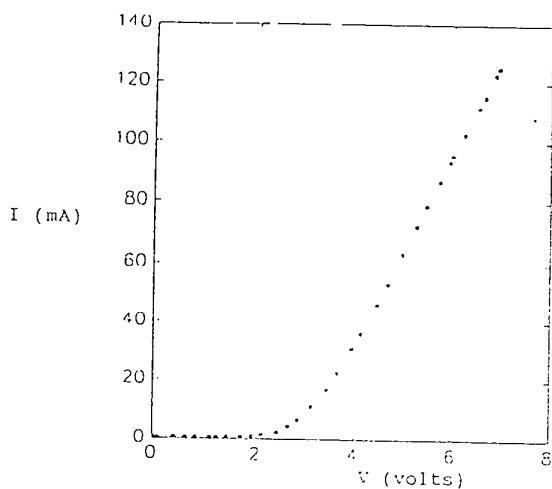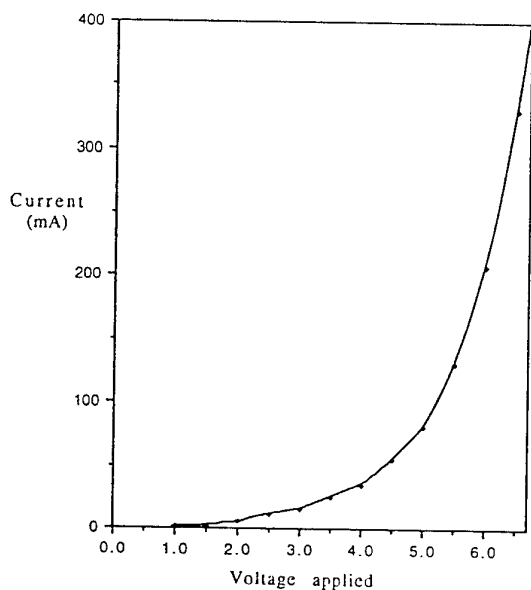
Fig. 1: MgIn/C$_{60}$ Schottky Diode

Fig.2: Ca/C$_{70}$ Schottky Diode

The most stable device produced was the n-Si/C$_{70}$ device. The main advantage of the n-Si/C$_{70}$ Schottky diode is its ease of fabrication. After full examination of its characteristics the device still worked well. The peak current of 108 mA was quite stable and reproducible over a period of weeks. A reference diode of Au/n-Si was prepared and showed a typical ohmic response, which would
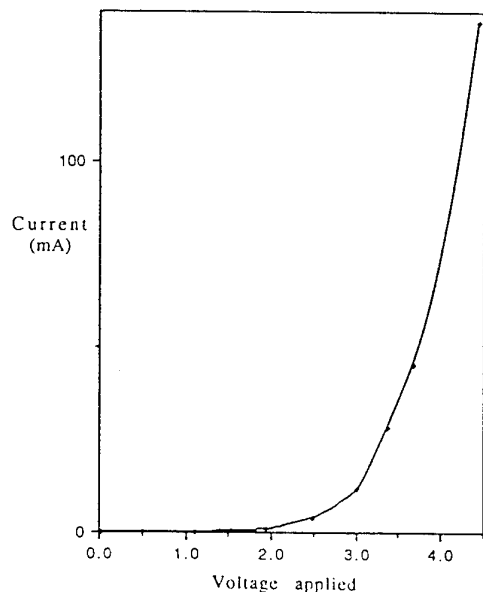
430

Fig. 3: Si/C_{70}
Schottky Diode

be expected from two materials which have low
resistivity. To ensure that the fullerenes formed a
Schottky diode with the low work function metals and not
the high ones, a sandwich layer was prepared consisting
of Au/C_{60}/Au and Au/C_{70}/Au. The result of this was a bulk
conductivity analysis. However, it did not form a
Schottky diode thus proving that the device
characteristics observed were indeed due to the Schottky
diode formed between low work function materials and the
fullerenes. Normally a p-type semiconductor makes a
Schottky contact with a low work function metal[6].
However if the Schottky contact is made utilising an n-
type semiconductor and a low work function metal this is
then due to a drift current induced by the minority
carriers.

Another important point to note is that the n-Si/C_{70} diode
shows a photovoltaic response shown in Fig.4. A short
circuit current of 1.5 A and an open circuit voltage of
106 mV is produced when exposed to 1 mW broadband light
intensity. The efficiency of this diode was in the region
of 0.1 but it is an indication of where fullerenes may be
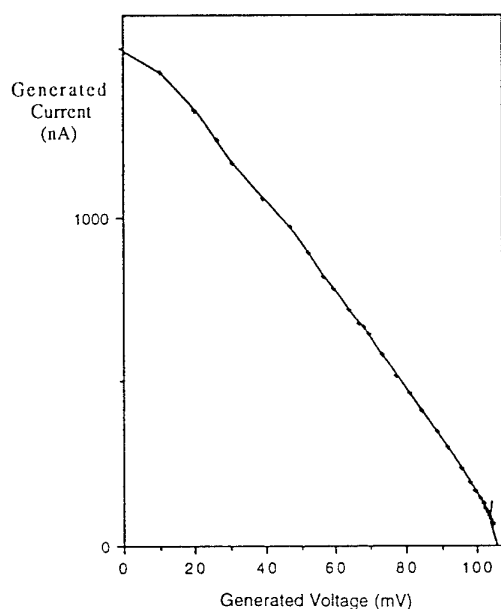made useful practically.

Fig. 4: Generated Current Voltage Characteristic of Si/C_{70}

Referenc

1. K.Pic
2. J.Kas
   Prope
   Solid
   Heide
3. J.Mor
   M.I.F
4. S.Ant
5. D.Bra
6. J.B.W
   (1991

5 Conclusion

The J vs V characteristics of fullerene devices all show Schottky diode behaviour which are quite stable and reproducible over a number of weeks. The diode behaviour is dominated by a drift current induced by the presence of the minority carriers and as a result the Schottky diode is formed at the low work function metal/fullerene interface. By calculating the barrier height at the junction between the metal and the semiconductor the electron affinity of both fullerenes is evaluated as 3.25 eV for C_{60}/Mg-In, 3.14 eV for C_{70}/Si and a more realistic value of 2.36 eV for C_{70}/Ca probably due to the better balancing of the metal contact work functions. As the more stable device produced was the n-Si/C_{70} it was studied for its photovoltaic ability. It produced a short circuit current of 1.5 μA and an open circuit voltage of 106 mV which was stable for a number of weeks.

References

1. K.Pichler, R.H.Friend: Synth. Met. 51(1992)257–265
2. J.Kastner, J.Paloheimo, H.Kuzmany: In Electronic
   Properties of High-T_c Superconductors, Springer Ser,
   Solid-State Sci., Vol.113 (Springer, Berlin,
   Heidelberg 1993) p.512
3. J.Mort, R.Ziolo, M.Machonkin, D.R.Huffman,
   M.I.Ferguson: Chem.Phys.Lett.186(1991)284
4. S.Anthoe, L.Tugula: phys.stat.sol. (a) 128,253(1991)
5. D.Braun, A.J.Heeger: Thin Solid Films 216(1992)96–98
6. J.B.Whitlock, P.Panayotatos: Thin Solid Films 205,
   (1991)69–75

ELSEVIER

Resonance Raman and infrared spectroscopy of carbon nanotubes

J. Kastner [a], T. Pichler [a], H. Kuzmany [a], S. Curran [b], W. Blau [b], D.N. Weldon [c],
M. Delamesiere [c], S. Draper [c], H. Zandbergen [d]

[a] *Institut für Festkörperphysik, Universität Wien, A-1090 Wien, Austria*
[b] *Department of Pure and Applied Physics, Trinity College, Dublin 2, Ireland*
[c] *Chemistry Department, Trinity College, Dublin 2, Ireland*
[d] *National Centre for HREM, Laboratory of Materials Science, Delft University, 2628 AL Delft, The Netherlands*

Abstract

We present a comparative analysis of the vibrational and structural properties of carbon nanotubes. The first-order Raman spectrum exhibits two lines at 1582 cm^{-1} and at 1350 cm^{-1}. The observed ratio of the integrated intensity of these lines was found to be different as compared to polycrystalline graphite. The position and intensity of the line around 1350 cm^{-1} strongly depend on the energy of the exciting laser line. This dispersion effect is again different from the dispersion in nanocrystalline graphite. It is discussed in terms of a photoselective resonance process. Transmission infrared spectra of the nanotubes show one broad and asymmetric line at 1575 cm^{-1} and a weaker line at 868 cm^{-1}.

1. Introduction

Since the discovery of the successful production of buckminster fullerene in macroscopic quantities, worldwide attention has focused on the unique properties of these molecules [1]. The recent discovery of even larger fullerenes, graphitic nanotubes [2] and onion-like polyhedra [3], has substantially increased the interest in this area. These new carbon materials are interesting both from a scientific and technological point of view. There might be practical applications in such diverse areas as high tensile strength fibres, molecular wires and solenoids [4]. The basic structure of nanotubes consists of one or usually more graphitic sheets wrapped around one another with a hollow core. The caps are usually closed by the presence of carbon pentagons. Consequently, the tubes contain no dangling bonds. This is an intrinsic difference to graphite crystallites where open bonds are at the edges. Due to this difference and due to the curved nature of the graphitic sheets in the tubes characteristically different vibrational properties can be expected. However, the difference to the properties of graphite crystallites might be rather small since both materials are nanoparticles. Moreover, the deviation from planarity is low in the graphitic sheets of a typical tube with more than a few nanometer diameter.

Monocrystalline graphite belongs to the D_{6h}^4 space-group symmetry [5–9]. The irreducible representation for the zone center optical modes is given by

$$\Gamma_{opt} = 2E_{2g} \, (R) + E_{1u} \, (IR) + 2B_{2g} + A_{2u} \, (IR) \, .$$

$$(1)$$

The E_{2g} modes are Raman active. One is a shear-type rigid-layer mode at 42 cm^{-1} and the other an in-plane stretching mode at 1582 cm^{-1} often designated as the G mode. The infrared optical vibrations are an out-of-plane A_{2u} mode at 868 cm^{-1} and an in-plane E_{1u}

mode at 1588 cm^{-1}. In polycrystalline graphite an additional line appears at 1350 cm^{-1} which can be assigned to phonons at the M and K points of the hexagonal Brillouin zone [5–7]. Since this line is disorder induced it is usually called the D line. Its second-order is of considerable intensity even in monocrystalline graphite because the phonon density of states has a maximum at 1350 cm^{-1}. Since the $k=0$ selection rule does not apply for second-order Raman scattering, phonons can be observed from any part of the Brillouin zone.

Raman spectra of carbon nanotubes [10] and closed-shell carbon particles [11] have been reported. A strong resemblance to the Raman spectrum of graphite was found. For carbon nanotubes the strongest Raman line is down-shifted by 6 cm^{-1} to 1574 cm^{-1} as compared to the E_{2g} mode of monocrystalline graphite. Additionally, a line at around 1350 cm^{-1} and its overtone at 2687 cm^{-1} have been observed.

In this Letter we present a correlation of the Raman spectrum of carbon nanotubes to their structural properties. Distinct differences between the resonance Raman behavior of carbon nanotubes, carbon microcrystallites and highly oriented pyrolytic graphite (HOPG) are discussed within a photoselective resonance picture. Finally, infrared (IR) spectra are presented and elucidated.

2. Experimental

The technique used to produce carbon nanotubes is similar to the one required for the production of fullerenes by using a steel fullerene generator. An 8 mm graphite rod of 99.99% purity and a plug of graphite were used as the positive and as the negative electrode, respectively. The generator was flushed with helium three times before evacuating to 450 Torr. A dc potential of 27 V was applied between the two graphite rods. After the positive electrode was consumed a cylinder with a grey outer layer and a black inner core was found on the negative electrode. This cylinder was placed in methanol and sonicated for ten minutes. This removed some of the inner black material from the cylinder to give a fine black suspension. After evaporating methanol a fine black powder was obtained containing approximately 70%

nanoparticles of which nanotubes are by far the most abundant. This was proven by high-resolution electron microscopy (HREM). Due to the high tube concentration it can be assumed that the Raman spectra are dominated by lines from the tubes. The rest of the material consisted of a fused mixture of tubes and polyhedra, and of amorphous carbon. No graphitic crystallites were observed. The nanotubes showed a distribution in length and diameter. Evaluating the electron micrographs yielded a distribution as shown in Fig. 1. For the length an effective value is plotted where the graphitic planes are not interrupted by dislocations or breaks. Both values, the length and the diameter, show a bimodal distribution peaking at 30 and 70 nm and 60 and 180 nm for the diameters and for the lengths, respectively. More detailed results of the HREM measurements will be published elsewhere [12].

Raman spectroscopy was performed using a Dilor XY spectrometer with a liquid-nitrogen cooled CCD detector. As excitation sources Ar$^+$, Kr$^+$ and a Ti:sapphire laser with wavelengths ranging from 457 up to 742 nm have been used. The measurements were taken in back-scattering geometry with a typical laser power of 1 mW (140 W/cm^2) and a spectral resolution of 2–4 cm^{-1}. Line positions and widths were obtained from a numerical fit using Lorentzian
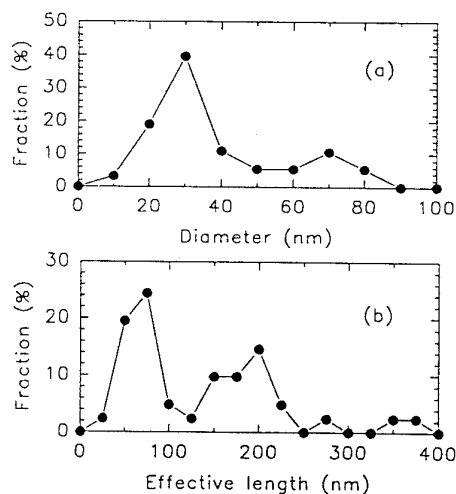

Fig. 1. Distribution in nanotube diameter (a) and effective length (b) as obtained by high-resolution electron microscopy. The total number of counted tubes was 350 and 60 for the diameter and the length, respectively.

line shapes. When conducting IR spectroscopy a mixture of 300 mg KBr and several milligrams of carbon nanotubes or graphite microcrystallites were prepared in pellet form. The pellets were placed in a Bruker IRS 66V spectrometer and transmittance spectra were taken between 400 and 5000 cm^{-1} with a resolution of 2 cm^{-1}. IR spectra of highly oriented pyrolytic graphite (HOPG) were taken from cleaved surfaces in reflexion 11° from normal incidence.

3. Results and discussion

3.1. Raman scattering

Fig. 2 shows Raman spectra in selected spectral regions of carbon nanotubes, graphite microcrystallites and HOPG after excitation with 457 nm. The strongest Raman line of all three studied materials has its maximum at 1582 cm^{-1}. It is the above mentioned G line. The full width at half maximum (fwhm) of this line is about 20–22 cm^{-1} for both nanotubes and graphite crystallites which is only slightly higher than that for HOPG (about 15–18 cm^{-1}). There is an additional line at 1350 cm^{-1} in the spectra of nanotubes and graphite microcrystallites assigned as the D line in Fig. 2. This line has the same intensity in both spectra.

The high-frequency part of the spectrum for all three materials studied is dominated by a strong line D* at around 2700 cm^{-1} which is the second-order of the D line. In the spectrum of HOPG this line consists of a doublet structure whereas in the other two

cases it is a single line. The D* line is much broader for crystallites (fwhm ≈ 71 cm^{-1}) and up-shifted ($\nu = 2742$ cm^{-1}) as compared to nanotubes (fwhm ≈ 49 cm^{-1} and $\nu = 2734$ cm^{-1}). In addition, there are several weak lines at 2455, 2955 and 3252 cm^{-1} in the second-order Raman spectra of all three materials. Since these lines are similar in shape and position for all studied materials they will not be discussed further. Raman lines at 100 and 860 cm^{-1} as calculated by Al-Jishi et al. [13] could not be observed. These new modes were predicted for tubes with a diameter of 2 nm. Since all observed tubes in our sample have a considerably large diameter, these additional Raman modes are expected to have vanishing intensity. In order to find the new nanotube modes future studies must concentrate on smaller tubes.

The D line is of considerable diagnostic significance because the ratio between its integrated intensity and the integrated intensity of the G line ($R = I_D/I_G$) depends on the structure of the studied carbon material. The in-plane graphite crystallite size L can be related to this ratio as [5–7]

$$L \text{ (nm)} = 4.4 \frac{I_G}{I_D}. \qquad (2)$$

This relation is valid for $0.001 \leqslant R \leqslant 1$ and for laser excitation between 488 and 514 nm. Since in our case R is 0.23 and thus in the range of validity of Eq. (2) the latter gives a nanotube length of 20 nm. This is a factor of 3 or 9 lower than the average obtained from HREM for the two peaks in the bimodal distribution. Since the concentration of contaminants like polyhedra is very low in our samples, this discrepancy must have structural reasons. We suggest the curved nature of the graphitic layers leads to an enhancement of the D line due to an enhancement of the electron–phonon coupling. Since it is generally accepted that the electron–phonon coupling increases by a σ admixture to the sp^2 bonded carbon atoms the present explanation seems plausible. Applying this interpretation to lower and larger size tubes means that the intensity of the D line will decrease with increasing diameter of the carbon nanotubes and approach for big tubes the value known from polycrystalline graphite before it finally disappears.

There are two further parameters which correlate to the graphite crystallite size: the band widths of the
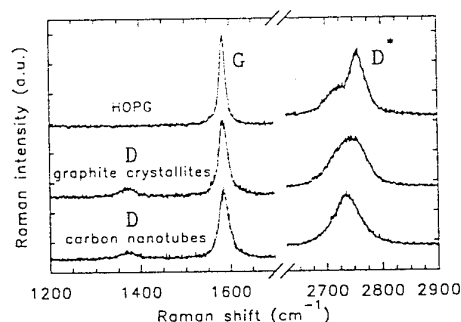

Fig. 2. Raman spectra of carbon nanotubes, graphite microcrystallites and highly oriented pyrolytic graphite (HOPG) as excited with 457 nm.

G and D* lines [5,7]. The smaller width of the D* line for tubes as compared to the one for crystallites is in accordance with the larger extension of the lattice along the direction of the tubes (nanotubes: $L = 130$ nm, graphite crystallites: $L = 20$ nm) and the enhancement of the D line for tubes due to their curved nature. From these considerations it can be concluded that the D* width versus crystallite size correlation is more or less identical for carbon nanotubes and polycrystalline graphite. However, the same width of the G line in both materials is at a first glance in contradiction to their different sizes. In order to understand it one has to take into consideration that the curved nature of nanotubes and their interplane disorder also lead to a line broadening. Hence the agreement of the widths for the G lines in tubes and in the crystallites is only by chance. The broadening mechanisms are completely different. The fact that only the G line for tubes and not the D* line is broadened might be related to the different origins of these lines. The G line is a zone center optical phonon, whereas the D* line is the second-order of a non-center phonon [7,9]. Calculations by Al-Jishi and Dresselhaus [9] showed that the low-energy side of the D* line dominantly comes from the K point and the high-energy side mainly from the M point. In the case of monocrystalline graphite and HOPG this gives a doublet structure with a shoulder at the low-energy side and in graphite crystallites a broadened single line. In carbon nanotubes the D* line is almost at the same position as the shoulder of the D* line for HOPG. Thus, for carbon nanotubes contributions from the region near a K derived point dominate the D* line due to the particular structure.

3.2. Resonance Raman scattering

In Fig. 3 Raman spectra of carbon nanotubes excited with different laser lines are shown. The spectra are normalized to equal height of the G line. Actually, the Raman intensity increases from $\lambda = 742$ nm to $\lambda = 457$ nm. The change of the signal to noise ratio originates from the spectrometer response function which has a broad maximum between 500 and 700 nm and is rather low at $\lambda = 457$ nm. One can clearly see that both the D and D* lines are shifted to lower wavenumbers with increasing wavelength of the exciting laser whereas the position of the G line re-
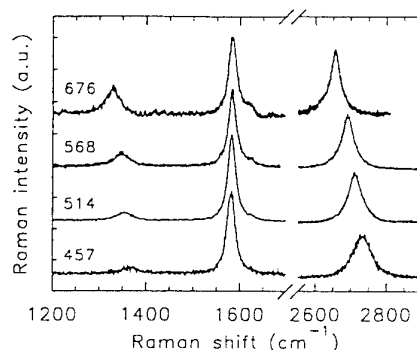

Fig. 3. Raman spectra of carbon nanotubes after excitation with different laser lines. The numbers indicate the wavelength in nm. The spectra were normalized so that the G lines have equal intensities in all cases.
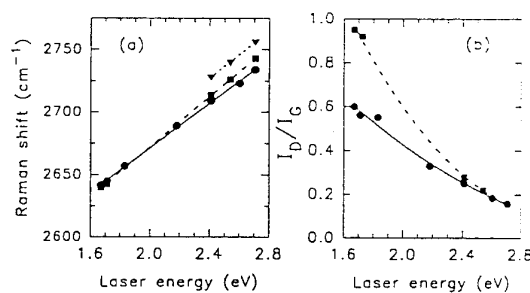

Fig. 4. Raman shift of the line around 2700 cm^{-1} (a) and integrated intensity of the D line as compared to the G line (b) for carbon nanotubes (●), graphite crystallites (■) and HOPG (▼) versus the energy of the exciting laser.

mains constant. The down-shift of the D* line (89 cm^{-1}/eV) is about twice as much as the one of the D line (43 cm^{-1}/eV). This is good proof that the D* line is really the second-order of the D line. In addition, a new line at 1620 cm^{-1} appears in the spectrum after excitation with the yellow or red laser. This line was also observed in the spectrum of graphite crystallites and similarly to the D line it was assigned to disorder-induced symmetry breaking by the microscopic particle size [14,15]. As with the D line the phonon density of states has a maximum at this energy. For the case of the tubes the disorder originates from the finite tube size and thus the interpretation for the origin of the line corresponds.

Fig. 4a shows explicitly the Raman shift of the D* line with the energy of the exciting laser line for all three studied samples. For HOPG only the position

of the high-energy line of the doublet is plotted. The D* line shift to higher wavenumbers is by about 15% weaker for carbon nanotubes as compared to graphite crystallites. The change of the relative intensities with the energy of the exciting laser is significant. The D line is much stronger as compared to the G line for excitation with the red laser as compared to excitation with the green or blue laser (Fig. 3). This is demonstrated in Fig. 4b. Here the intensity ratios of the D line to the G line are plotted versus the energy of the exciting laser for nanotubes and microcrystallites. This ratio decreases non-linearly with increasing laser energy and behaves characteristically different for tubes and graphite crystallites.

A dependence of the Raman shift of a mode on the energy of the exciting laser is formally called a dispersion effect. There are several possible explanations for this behavior.

It might be related to a probing of the sample at different depths below the surface as known from inorganic semiconductors [16]. This would require a depletion of carriers at the surface to the depth of the penetrating light. Since the tubes studied here are rather large they have a narrow electronic gap [4] and thus at room temperature a high carrier concentration. This situation is not compatible with a large depletion depth which consequently rules out this mechanism.

The dispersion might then be rather attributed to a photoselective resonance process. Two different mechanisms are possible for the tubes.

Similarly, as in conjugated polymers and sp-bonded linear carbon molecules [17–19] force constants, frequencies and electronic transitions may depend on the size of the nanotubes. By measuring with different laser energies one is probing selectively different parts of the sample and the overall response gives the resulting line shape and line position. Calculations showing an increase in the band gap with decreasing size for at least some of the tubes [4] are in agreement with this hypothesis. However, within this picture the independence of the line shift on the crystallite size is hard to explain. Therefore, another model may work better. The line shifting can be related to the dispersion of the D phonon at the Brillouin zone edge at the M and K derived points [14]. Excitations with different laser energies will result in different resonance enhancements of the contributions from

regions near the K and M derived points to the D line.

In both photoselective resonance pictures the special electronic structure of carbon nanotubes accounts for the difference in the dispersion as compared to graphite.

A change in the I_D/I_G ratio with the energy of the exciting laser for different forms of polycrystalline graphitic materials was already observed by several authors [14,20,21]. It was attributed to a stronger resonance enhancement of the G line as compared to the D line [21]. By excitation with a red laser one is far away from the $\pi–\pi^*$ transition (4–5 eV) and the G line is no longer more enhanced as compared to the D line. Applying this model to the results presented here reveals a difference in the resonance Raman profile for graphite and carbon nanotubes. This shows again that the electronic structure of carbon nanotubes is characteristically different from graphite and graphite microcrystallites.

3.3. Infrared spectroscopy

The IR spectra in selected spectral regions are shown in Fig. 5 for carbon nanotubes, graphite microcrystallites and HOPG. The spectra of nanotubes and microcrystallites have been measured in transmission using KBr pellets, whereas the spectrum of HOPG has been measured on an 11° tilted and cleaved surface in reflexion. For the presentation the background of all spectra was subtracted. This back-
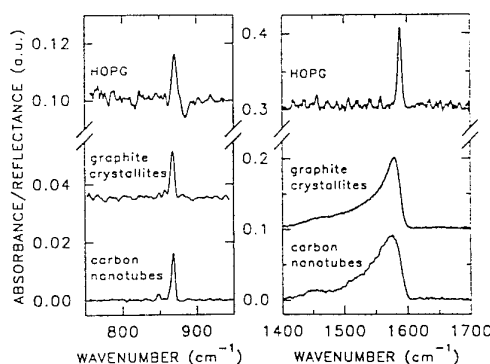

Fig. 5. Transmission infrared spectra in selected energy regions of carbon nanotubes and graphite microcrystallites. The infrared spectrum of HOPG measured in reflexion is included in the upper part of the figure.

ground was $100\times$ larger than the line at $860\ cm^{-1}$ and $1000\times$ larger than the line at $1587\ cm^{-1}$.

The IR spectrum of HOPG shows the two known lines at 868 (A_{2u}) and $1587\ cm^{-1}$ (E_{1u}), which is in good agreement with the results by Nemanich et al. [7,8]. The IR spectra for both carbon nanotubes and graphite crystallites are different from the one for HOPG, but resemble each other strongly. The A_{2u} mode is at the same position as in HOPG whereas the E_{1u} mode is softened to about $1575\ cm^{-1}$ and considerably broadened with an asymmetric tail in the low-energy region.

The shift of the E_{1u} mode can have several reasons. Firstly, a change of the interplane bonding leads to a change of the E_{1u} line because its energy is associated with an interlayer force constant. Moreover, introduced disorder and finite size effects may lead to a line broadening and shifting as well. Finally, the bending of the graphitic sheets might lead also to the same effect. Probably all mechanisms contribute to the observed shape and position of the E_{1u} mode.

4. Conclusion

Carbon nanotubes have been characterized by high-resolution electron microscopy, resonance Raman and IR spectroscopy. It has been shown that the I_D/I_G ratio versus the in-plane graphite sheet size of carbon nanotubes is different from the corresponding relation in polycrystalline graphite. Due to the curved nature of the graphitic sheets the electron–phonon coupling constant and therefore also the D line is enhanced. A dispersion and resonance effect was found for the D line. The discrepancy between carbon nanotubes and graphite microcrystallites has been attributed to different resonance Raman profiles and their different electronic structure. IR spectra of carbon nanotubes have been presented. The difference to the spectrum of HOPG has been explained by disorder induced line broadening and softening.

References

[1] W. Krätschmer, L.D. Lamb, K. Fostiropoulos and D. Huffmann. Nature 347 (1990) 354.
[2] S. Iijima. Nature 354 (1991) 56.
[3] D. Ugarte. Nature 359 (1992) 707.
[4] M.S. Dresselhaus, G. Dresselhaus and P.C. Eklund, J. Mater. Res. 8 (1993) 2054.
[5] D.S. Knight and W.B. White, J. Mater. Res. 4 (1989) 385.
[6] F. Tuinstra and J.L. Koenig, J. Chem. Phys. 53 (1970) 1126.
[7] N.B. Brandt, S.M. Chudinov and Ya. G. Ponomarev. Graphite and its compounds (North Holland, Amsterdam, 1988).
[8] R.J. Nemanich, G. Lucovsky and S.A. Solin, Solid State Commun. 23 (1977) 177.
[9] R. Al-Jishi and G. Dresselhaus. Phys. Rev. B 26 (1982) 4514.
[10] H. Hiura, T.W. Ebbesen, K. Tanigaki and H. Takahashi, Chem. Phys. Letters 202 (1993) 509.
[11] W.S. Bacsa, W.A. de Heer, D. Ugarte and A. Chatelaun, Chem. Phys. Letters 211 (1993) 346.
[12] D. Weldon, W. Blau, H. Zandbergen, S. Draper and M. Delamesiere. to be published.
[13] R. Al-Jishi, L. Venkataraman, M.S. Dresselhaus and G. Dresselhaus. Chem. Phys. Letters 209 (1993) 77.
[14] R.P. Vidano, D.B. Fischbach, J. Willis and T.M. Loehr, Solid State Commun. 39 (1981) 341.
[15] K. Nakamura, M. Fujitsuka and M. Kitajima, Phys. Rev. B 41 (1990) 12260.
[16] G. Abstreiter, M. Cardona and A. Pinczuk, in: Light scattering in solids, Vol. 4, eds. M. Cardona and G. Güntherodt (Springer, Berlin, 1984).
[17] H. Kuzmany. Phys. Stat. Sol. b 97 (1980) 521.
[18] H. Kuzmany and J. Kastner, in: Macromolecules 1992, ed. J. Kahovec (VSP, Zeist, 1993) 333.
[19] J. Kastner, H. Kuzmany, L. Kavan, F. Dousek and J. Kürti, J. Chem. Phys., submitted for publication.
[20] T.P. Mernagh, R.P. Cooney and R.A. Johnson, Carbon 22 (1982) 39.
[21] K. Sinha and J. Menendez, Phys. Rev. B 41 (1990) 10845.